Chapter 3
Interface Engineering for High Performance Bulk-Heterojunction Polymeric Solar Cells

Chunhui Duan, Chengmei Zhong, Fei Huang and Yong Cao

Abstract The nature of electrical contact between the bulk-heterojunction (BHJ) layer and the electrodes is critical to the overall performance and stability of polymer solar cells (PSCs). In recent years, considerable efforts have been devoted to the interface engineering of BHJ–PSCs. In this chapter, we reviewed the development of interface modification materials and their applications in BHJ–PSCs. The discussions were divided into several sections according to the device configuration of BHJ–PSCs, i.e., conventional device, inverted device, and tandem device. For single junction devices (including conventional and inverted devices), we highlighted the interface modification materials which were applied at both electron-collecting and hole-collecting electrodes, including inorganic materials (such as metals, salts, semiconducting oxides, etc.), self-assembled monolayers (SAMs) or SAMs-modified functional layers, and organic/polymeric materials. For tandem devices, the discussions were focused on the functional materials utilized as intermediate connectors. As discussed in this chapter, the development of interface modification materials has resulted in great progress in BHJ–PSCs, which can potentially pave the way for the commercialization of BHJ–PSCs.

3.1 Introduction

Bulk-heterojunction (BHJ) polymer solar cell (PSC) is one of the most promising photovoltaic techniques to directly convert the terrestrial solar radiation into electricity because of their compatibility with low-cost, large-scale fabrication by

C. Duan · C. Zhong · F. Huang (✉) · Y. Cao
State Key Laboratory of Luminescent Materials and Devices, Institute of Polymer
Optoelectronic Materials and Devices, South China University of Technology,
Guangzhou 510640, P. R. China
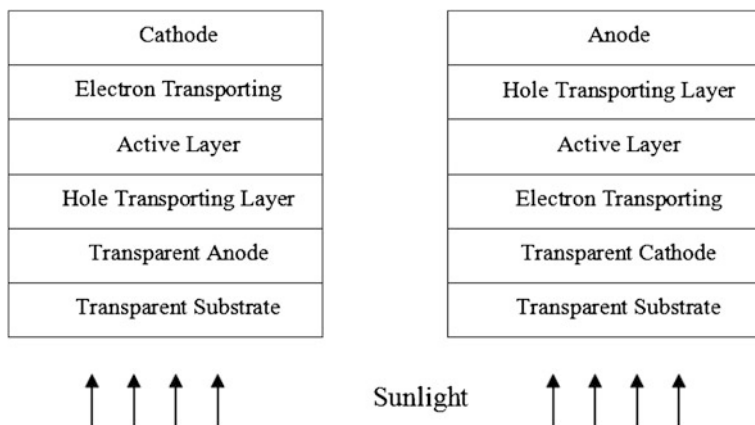e-mail: msfhuang@scut.edu.cn

Cathode	Anode
Electron Transporting	Hole Transporting Layer
Active Layer	Active Layer
Hole Transporting Layer	Electron Transporting
Transparent Anode	Transparent Cathode
Transparent Substrate	Transparent Substrate

↑ ↑ ↑ ↑   Sunlight   ↑ ↑ ↑ ↑

Fig. 3.1 Comparison of conventional device structure (*left*) and inverted device structure (*right*) for BHJ–PSCs

solution processing [1–3]. In the last two decades, great progress in the field of BHJ–PSCs has been achieved with the power conversion efficiency (PCE) increasing from around 1 % to more than 9 % [4]. Such great advancement was driven by the efforts in various aspects including the development of new low-band-gap conjugated polymers and new fullerene-based acceptor materials [5–7], the usage of new device processing methods [8–10], the invention of new device structures [11, 12], the application of innovative interface modification materials [13–15], and so forth. The simplest structure of BHJ–PSC is the so-called sandwich device structure, where the blend of conjugated polymer donor and fullerene derivative acceptor was sandwiched between a transparent metal oxide, such as indium tin oxide (ITO), and a metal electrode [16]. For conventional devices, ITO and low work-function metal are used as anode and cathode, respectively. While in an inverted device, the modified ITO and high work-function metal are cathode and anode, respectively. The configurations of conventional and inverted device for BHJ–PSCs are demonstrated in Fig. 3.1. It is well-known that the nature of electrical contact between the organic active layer and the electrodes is critical to the overall device performance, for both the conventional and inverted devices [13–15]. The ideal Ohmic contact in the organic blend layer/electrode interface with an energy barrier height as low as possible is thus desired for efficient charge carrier extraction and transport, and thereby reduce the recombination loss caused by the accumulation of charge in the interface. Indeed, a barrier height of several tens of mV may lead to severe charge accumulation. Therefore, the modification of organic active layer/electrode interface is critical to achieve high efficiency and long-term stability for BHJ–PSCs. As a result, in recent years, a lot of efforts from research groups all around the world are devoted to the development of new interfacial materials with different functions and their applications. The aim is to achieve high PCE and long-term stability for BHJ–PSC devices [13–15].

In principle, ideal interfacial materials should first function as charge extraction or transporting layer to minimize the barrier height in organic active layer/electrode interfaces, which will help to form Ohmic contact in interface to reduce recombination loss and consequently obtain enhanced short circuit current density (J_{sc}). Additionally, this layer should also function as exciton blocking layer to selectively transport only one type of carrier and block the other, i.e., an electron extraction/transporting layer with hole blocking property, and a hole extraction/transporting layer with electron-blocking ability. Moreover, the interfacial layer usually functions as buffer layer to prevent the chemical reaction between organic active layer and metal electrode, and the diffusion of metal ions into organic layer. Furthermore, it was found that some interfacial materials can also function as optical spacers to modulate the incident light distribution in BHJ–PSCs, so that the maximum incident light intensity located around the center of the active layer to ensure as much as incident light harvested by the device and consequently to obtain maximum J_{sc} [13, 15].

In this chapter, we will review interfacial materials applied at the interfaces between organic active layer and electrodes, including both anode and cathode, and their influence on the photovoltaic performance of BHJ–PSC devices. The design of interfacial materials and their applications will be divided into several sections by the device structure, including conventional device, inverted device, and tandem device. For single junction devices (including conventional and inverted devices), the interfacial materials applied at both cathode and anode will be separately reviewed in the categories of inorganic materials (including metals, salts, semiconducting oxides, etc.), self-assembled monolayers (SAMs) or SAMs modified functional layers, as well as organic/polymeric materials. For tandem devices, we will focus on the functional materials used as intermediate connectors.

3.2 Interface Engineering for Conventional Solar Cell Devices

3.2.1 Cathode Interlayer

For a conventional BHJ–PSC, the efficient electron extraction at cathode is of critical importance for the high J_{sc} and the overall photovoltaic performance. Aluminum (Al) is a most widely used electrode materials for BHJ–PSCs because of its abundance and proper work function of 4.3 eV, which is very close to the lowest unoccupied molecular orbital (LUMO) energy levels of acceptor materials such as (6,6)-phenyl-C_{61}-butylric acid methyl ester ($PC_{61}BM$) and (6,6)-phenyl-C_{71}-butylric acid methyl ester ($PC_{71}BM$) (see Scheme 3.1). However, the organic optoelectronic devices with Al cathode usually suffer from poor stability, because the reactive hot Al atoms generated at the thermal evaporation process can diffuse into the organic layer and result in chemical reaction at the metal/organic interface [17, 18]. Moreover, it was reasoned that Al–C bond formation at the Al/organic
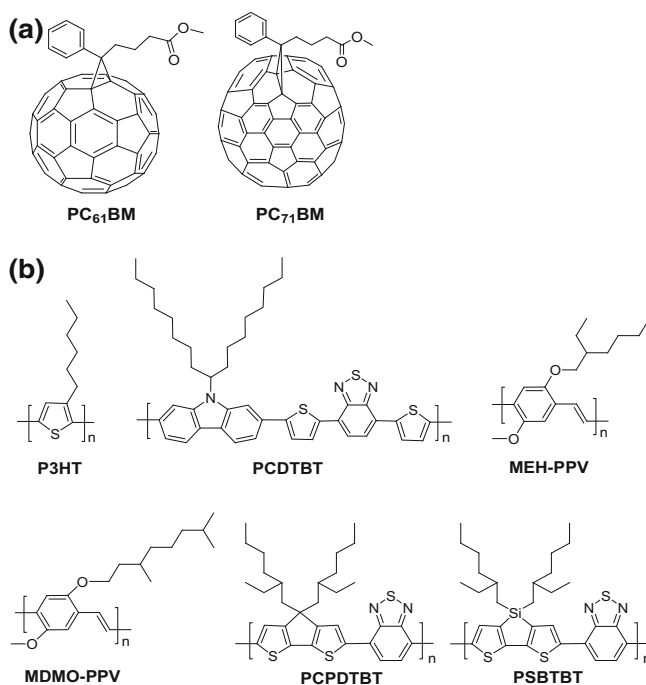
Scheme 3.1 Chemical structures of the most widely used (**a**) acceptors (PC$_{61}$BM and PC$_{71}$BM) and (**b**) donors (P3HT, PCDTBT, MEH-PPV, MDMO-PPV, PCPDTBT, and PSBTBT)

interface can inevitably break the π-conjugated system of organic layer, and thereby lead to poor stability of Al cathode [19, 20]. Hence, various interfacial materials were inserted into the organic active layer/Al junction to improve the interface contact properties and thereby photovoltaic performance of BHJ–PSCs. The summary of performance of conventional PSCs using different cathode interlayer designs are listed in Table 3.1 and the chemical structures of organic materials used as cathode interlayer in conventional PSCs are shown in Scheme 3.2.

3.2.1.1 Metal and Inorganic Compounds as Cathode Interlayer

Low work-function metals, such as calcium (Ca) or barium (Ba), which were two widely used interfacial materials for polymeric light-emitting diodes (PLEDs) [21, 22], were also usually inserted into the interface between Al and organic active layer to further improve the device performance via the formation of ideal Ohmic contact at interface. The BHJ–PSCs with a thin layer of Ca or Ba between Al and organic active layer usually exhibited superior device performance, especially open circuit voltage (V_{oc}) with respect to PSCs with bare Al as cathode.

Table 3.1 Summary of device characteristics of representative conventional PSCs employing different cathode interlayers

Cathode	Anode	Active layer	PCE	J_{sc} (mA cm^{-2})	V_{oc} (V)	FF	Ref
Ca/Al	ITO/PEDOT:PSS	P3HT:PC$_{61}$BM	4.37	10.60	0.61	0.67	[9]
LiF/Al	ITO/PEDOT:PSS	MDMO-PPV:PC$_{61}$BM	2.50	5.25	0.82	0.61	[23]
Cs$_2$CO$_3$/Al	ITO/PEDOT:PSS	P3HT:PC$_{61}$BM	3.10	9.50	0.56	0.60	[30]
TiO$_x$/Al	ITO/PEDOT:PSS	P3HT:PC$_{61}$BM	5.00	11.10	0.61	0.66	[36]
TiO$_x$/Al	ITO/PEDOT:PSS	PCDTBT:PC$_{71}$BM	6.10	10.60	0.88	0.66	[37]
ZnO/SAM/Al	ITO/PEDOT:PSS	P3HT:PC$_{61}$BM	4.21	11.61	0.65	0.55	[40]
PEO/Al	ITO/PEDOT:PSS	APFO-5:PC$_{61}$BM	1.84	4.00	0.90	0.51	[45]
PFNBr-DBT15/Al	ITO/PEDOT:PSS	PFO-DBT35:PC$_{61}$BM	1.9	3.9	0.95	0.39	[48]
WPF-6-oxy-F/Ag	ITO/PEDOT:PSS	P3HT:PC$_{61}$BM	3.69	9.86	0.64	0.58	[52]
PFN/Al	ITO/PEDOT:PSS	PECz-DTQx:PC$_{71}$BM	6.07	11.4	0.81	0.66	[54]
PF-b-P3TMAHT/Al	ITO/PEDOT:PSS	PCDTBT:PC$_{71}$BM	6.2	10.6	0.89	0.67	[56]
SnCl$_2$Pc/LiF/Al	ITO/PEDOT:PSS	MEH-PPV:PC$_{61}$BM	2.49	6.77	0.82	0.45	[57]
F-PCBM/Al	ITO/PEDOT:PSS	P3HT:PC$_{61}$BM	3.79	9.51	0.57	0.70	[58]
PDMS-b-PMMA/Al	ITO/PEDOT:PSS	P3HT:PC$_{61}$BM	3.86	9.61	0.60	0.67	[59]
P(VDF-TrFE)	ITO/PEDOT:PSS	P3HT:PC$_{71}$BM	4.5	12.8	0.589	0.60	[61]

However, both Ca and Ba are active metals, and thus are sensitive to the moisture in the ambient atmosphere. Although the stability of the solar cell devices could be improved in some degree by depositing a thick layer of Al or Ag onto Ca or Ba to
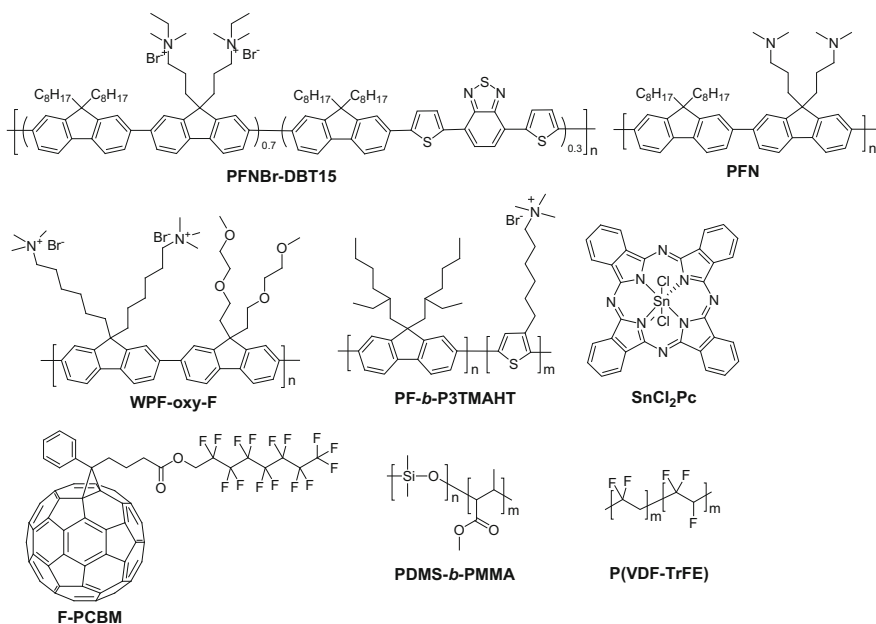
Scheme 3.2 Chemical structures of organic materials for cathode interlayer

form bilayer cathodes, such as Ca/Al and Ba/Al, the development of new inter-facial materials to use as cathode interlayer is still required.

Inorganic fluorides, such as lithium fluoride (LiF), are promising electron extraction materials for BHJ–PSCs. A bilayer electrode of LiF/Al is usually chosen to replace a pristine Al cathode, because a thin layer of LiF can guarantee a good Ohmic contact between the metal and the organic active layer [23]. The formation of a favorable dipole moment or a LiF buffer layer at the organic active layer/LiF/Al interface is usually considered to be the reason why LiF could improve the performance of BHJ–PSCs. It was considered that a monolayer covered LiF can be decomposed upon Al deposition and resulting in Li-doping of the organic layer to deliver a low work-function contact; while a thick LiF usually generates a dipole layer to lower the work function of electrode [24–26].

Caesium carbonate (Cs_2CO_3) is another efficient electron extraction material used to fabricate bilayer cathode for BHJ–PSCs [27, 28]. Interestingly, the Cs_2CO_3 layer can be deposited by either thermal evaporation or solution spin coating. The implementation of Cs_2CO_3 is beneficial for reducing the electron extraction barrier and series resistance (R_s). Compared to bare Al device, the device with inserted Cs_2CO_3 exhibited enhanced V_{oc} and fill factor (FF) [29, 30]. However, whether the actual product of thermally evaporated Cs_2CO_3 is Cs_2O or Cs_2CO_3 is still uncertain[27, 31–33]. Anyway, it is widely accepted that the formation of Al–O–Cs complex yields the low work-function contact and thus facilitates the electron extraction [27].

n-Type semiconducting metal oxides such as titanium suboxide (TiO_x), which is a well-known photocatalyst and is widely used in dye-sensitized solar cells [34, 35], had attracted considerable attention recently due to its solution pro-cessability from sol to gel process [36], nontoxicity, and transparency. TiO_x possesses a conduction band edge and valence band edge of -4.4 and -8.1 eV, respectively, which would endow TiO_x good electron extraction ability from active layer and outstanding hole-blocking ability [36]. Hence, TiO_x is an ideal cathode modification material for BHJ–PSCs application [36]. The TiO_x layer can also resist the permeation of oxygen and moisture into the organic active layer, because the formation of robust titanium oxide film via annealing the titanium oxide film deposited by sol–gel process at 150 °C. Moreover, the TiO_x layer can also function as an optical spacer via spatially redistributing the incident light intensity to further improve the light harvesting property of BHJ–PSCs [36]. Recently, Park et al. reported a promising PCE of 6.1 % for BHJ–PSCs with poly[N-9′-heptadecanyl-2,7-carbazole-alt-5,5-(4′,7′-di-2-thienyl-2′,1′,3′-benzothiadiazole)] (PCDTBT, see Scheme 3.1):$PC_{71}BM$ blend as active layer by inserting TiO_x as an electron extraction layer and optical spacer. Notably, the device exhibited internal quantum efficiency (IQE) closing to 100 % around 450 nm, which indicates the high effi-cient conversion of incident photon into charge carrier [37]. However, the intrinsic electrical properties of the TiO_x film are dominated by the processing conditions. Additionally, the electron mobility of TiO_x is 1.7×10^{-4} cm^2 V^{-1} s^{-1}, which is almost two orders of magnitude lower than that of $PC_{61}BM$, and this may

potentially limit the device performance. To further improve the property of a TiO_x interlayer, Park et al. fabricated Cs-doped film TiO_2 by mixing Cs_2CO_3 solution with a nanocrystalline TiO_2 solution prepared from a sol to gel process. The work function of TiO_2 was successfully downshifted by Cs doping to yield a better Ohmic contact between organic active layer and metal electrode. The improved electron extraction combining the preserved hole-blocking ability of the TiO_x interlayer afforded a much better photovoltaic performance for the poly(3-hexylthiophene) (P3HT, see Scheme 3.1)/$PC_{61}BM$ solar cell than that of cell using sole TiO_x interlayer [38].

ZnO is another *n*-type metal oxide, which possesses a high electron mobility of 0.066 cm^2 V^{-1} s^{-1} [39] and a Fermi level of 4.4 eV [40]. The high electron mobility, ideal Fermi level, and solution processability of ZnO nanoparticles (NPs) indicate that ZnO would be a good interfacial material to facilitate not only the efficient charge transfer from $PC_{61}BM$ (or $PC_{71}BM$) to ZnO, but also the effective electron collection at cathode. In addition, the wide band gap of ZnO (3.2 eV) would endow it good hole blocking ability and good transparency. Moreover, Gilot et al. had proved that ZnO can also serve as an effective optical spacer for thin (<60 nm) active layers [41]. These advantages of ZnO render its widely application in inverted BHJ–PSCs. However, the direct use of ZnO as cathode buffer layer for conventional PSCs is scarce.

3.2.1.2 Self-Assembled Monolayer on Metal Oxide Surface

The contact property of ZnO/metal bilayer cathode and resulted device performance could be further improved by spin coating the functional SAM on the ZnO surface [42, 43]. Modifying the ZnO NPs surface with a benzoic acid group constituted with electron donating end groups (such as $-OCH_3$, $-CH_3$, $-H$), which form a negative dipole (toward metal and away from ZnO), the band offset between the conduction band of ZnO and the work function of metal can be decreased, and thereby the Ohmic contact was formed. Compared to the unmodified devices, the devices with SAMs-modified ZnO NPs interlayers showed significant improvement in all the *J–V* characteristics including J_{sc}, V_{oc}, FF, and PCE. On the other hand, opposite effect was observed when the ZnO NPs layer was modified with electron-withdrawing end groups substituted SAM molecules [40]. PCE of 4.2 % was achieved for device with SAM modification with respect to 3.2 % for the control device with unmodified cathode [40]. A further enhanced PCE of 4.6 % was obtained when the ZnO NPs layer was modified with captoundecanoic acid [44]. More importantly, the stable high work-function metals such as Ag and Au can also be used as cathodes, and the PCE of 3.65 % and 3.22 % were achieved for P3HT:$PC_{61}BM$ devices with ZnO/SAM/Ag and ZnO/SAM/Au cathodes, respectively [40].

3.2.1.3 Water/Alcohol Soluble Polymers as Cathode Interlayer

Although the above-mentioned inorganic materials exhibited outstanding cathode modification functions, the thermal evaporation of most of them requires high vacuum, which leads to increases in fabrication costs and thereby limits their applications. Organic interfacial materials were thus widely developed to improve the interface property of metal electrode, because of their solution processability, facile modification of chemical structures, and in turn electrical and electronic properties. The commonly used organic interfacial materials for cathode modification are summarized in Scheme 3.2. Zhang et al. had reported the use of environment friendly aqueous solution processable poly(ethylene oxide) (PEO) as interlayer to modify the cathode in BHJ–PSCs, which showed similar function as LiF. The PSCs with PEO modified cathode showed not only enhanced V_{oc}, but also J_{sc} and FF [45].

Water/alcohol soluble conjugated polyelectrolytes (CPEs) and related neutral polymers, which bear pendant hydrophilic polar groups, were widely used as promising interfacial materials in organic optoelectronic devices such as polymer light-emitting diodes, field effect transistors (FETs), and solar cells. Their special solubility in environment friendly solvents such as alcohol and water provide the convenience of fabricating multilayer organic devices by avoiding the problem of corrupting the low-lying neutral organic semiconducting layers which are usually dissolved in nonpolar solvents. It was generally considered that the interfacial dipoles were formed by inserting a CPE layer, and thereby the reduction of electron extraction barrier to electron collection and transporting at cathode. In addition, UV photoelectron spectroscopy has shown that this kind of polymers can effectively influence the work function of adjacent electrodes. Moreover, a large amount of water/alcohol soluble fluorene-based CPEs and related neutral polymers were successfully used as electron injection/transporting materials in PLEDs [46, 47]. Luo et al. reported the use of a thin layer of alcohol-soluble fluorene-based CPE PFNBr-DBT15 between the active layer and metal electrode, and the V_{oc} of the resulted PSCs can be enhanced by 0.3 V [48]. Based on Luo's work, He et al. has insightfully investigated five different alcohol-soluble fluorene-based conjugated polymers or CPEs as cathode interlayers for PSCs based different donor materials system. He's results revealed that the V_{oc} enhancement is only observed in devices that contain a polyfluorene copolymer as the donor material, while no significant enhancement in V_{oc} was found for P3HT and poly(2-methoxyl-5-((2′-ethylhexyl)oxyl)-1,4-phenylenevinylene) (MEH-PPV, see Scheme 3.1) devices [49]. Similar works of using other fluorene-based alcohol polymers as interfacial materials for cathode modifications were also demonstrated by Na et al. and Zhao et al. almost at the same time [50, 51]. Notably, BHJ–PSCs with high work-function metals such as Ag, Au, and Cu also showed encouraging device performances with PCE above 3 % with the implementation of fluorene-based CPE WPF-6-oxy-F [52]. After that, the use of alcohol-soluble conjugated polymer as cathode interlayer gradually become a commonly applied approach to further improve the performance of PSCs [53, 54], and the encouraging PCE of 6.07 %

was achieved by inserting a thin layer of PFN (see Scheme 3.2) for the BHJ–PSC based on a newly developed low-band-gap donor material [54]. Recently, new water-/alcohol-soluble conjugated polymers and ionic conjugated di-block copolymer based on carbazole or thiophene were also developed to use as cathode interfacial materials [55, 56]. Compared to the device with sole Al as cathode, the PCE of PSCs can be enhanced from 5 to 6.5 % by inserting an ultra-thin, ionic conjugated, di-block copolymer poly[9,9-bis(2-ethylhexyl)-fluorene]-*b*-poly[3-(6-trimethylammoniumhexyl)thiophene] (PF2/6-b-P3TMAHT) [56]. These encouraging results indicate that water-/alcohol-soluble conjugated polymers would be good candidates of cathode interfacial materials for the future development of printable large-scale solar cells.

3.2.1.4 *n*-Type Organic Semiconductors as Cathode Interlayer

n-Type organic semiconductors having low-lying LUMO levels, which are close to the LUMO of $PC_{61}BM$ and the work function of Al cathode, are potentially electron extraction and transporting materials for BHJ–PSCs. Recently, Zuo et al. had reported the use of *n*-type phthalocyanine tin (IV) dichloride ($SnCl_2Pc$) as cathode interlayer to form $SnCl_2Pc$/LiF/Al trilayer cathode for PSCs. The integration of $SnCl_2Pc$ into the solar cell not only enhances the electron transporting and collection efficiencies due to the step-like electron injection barrier to cathode after the implementation of $SnCl_2Pc$ interlayer, but also improves the exciton dissociation efficiency because of the formation of additional MEH-PPV/$SnCl_2Pc$ exciton dissociation junction. Consequently, the 15.2 % enhancement of PCE up to 2.49 % was achieved for PSCs with the thermally evaporated $SnCl_2Pc$ as cathode interlayer [57].

3.2.1.5 Organic Cathode Interlayer Formed by Surface Self-Segregation

Compared to the thermal evaporation, the formation of a interfacial layer of *n*-type organic semiconductor by controlling the surface segregation of the materials during spin coating may be a much milder approach for the low-lying organic active layer. Wei et al. had reported that when a small amount of a fullerene derivative with a fluorinated alkyl chain (F-PCBM) is mixed with the blend of P3HT and $PC_{61}BM$, the F-PCBM spontaneously migrates to the surface of the organic layer during spin coating due to the low surface energy of the fluorinated alkyl chain. The interfacial dipole moment toward the Al cathode caused by the perfluoroalkyl chains is favorable for the reduction of the work function of Al for better alignment with $PC_{61}BM$ energy levels. The energy barrier for electron collection and the R_s of the modified device were hence reduced, and consequently the enhanced PCE of the device was achieved [58]. The surface self-segregation approach was also applied to incorporate a thin layer of poly(dimethylsiloxane)-*b*-poly(methylmethacrylate) (PDMS-*b*-PMMA) di-block copolymer at the interface between organic active layer

and Al electrode to function as a buffer layer for improving the performance of PSC. An enhancement of the PCE of the PSCs from 3.05 % to 3.56 % on average, and the highest PCE of 3.86 % were achieved by inserting a PDMS-*b*-PMMA into the P3HT:PC$_{61}$BM solar cells due to the reduction of charge carrier recombination at the organic/metal interface [59].

3.2.1.6 Ferroelectric Polymer as Cathode Interlayer

It is well-known that a sufficient intrinsic internal electric field is required to efficiently dissociate the charge transfer excitons generated in active layer [60]. However, most widely used electrode materials deliver a work function offset of <2 eV, affording a much smaller internal electric field for efficient charge transfer excitons dissociation in BHJ–PSCs [36]. Therefore, an external bias voltage is generally needed to efficiently dissociate the electrons and holes. Most recently, Yuan et al. demonstrated another innovative method to provide sufficient intrinsic internal electric field in BHJ–PSCs by inserting a ultra-thin ferroelectric polymer layer of vinylidene fluoride-trifluoroethylene copolymer (P(VDF-TrFE)) between organic active layer and Al electrode [61]. After poling, an induced net polarization electric field is generated, which is ten times-higher than that achieved by the use of electrodes with different work functions. As a consequence, an enhanced PCE from 1–2 % without the ferroelectric film to 4–5 % was demonstrated for BHJ–PSCs based on several different active layers. Also note that these improved PCEs are higher than those achieved by other methods, including active layer morphology and electrode work-function optimization [61].
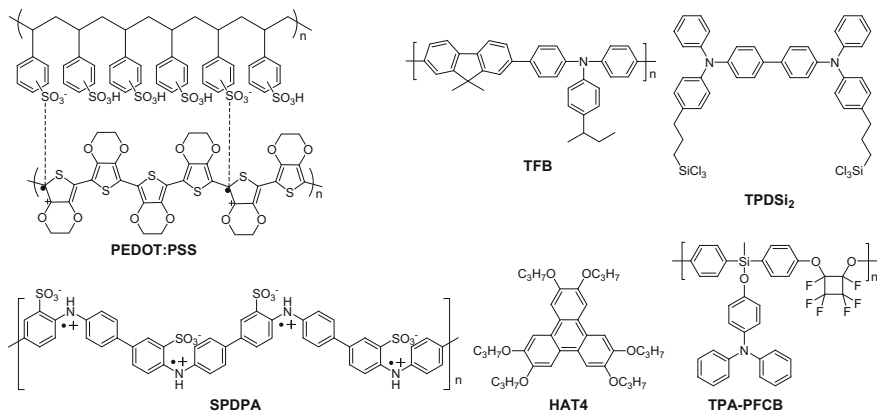
3.2.2 Anode Interlayer

3.2.2.1 PEDOT: PSS as Anode Interlayer

Interface engineering at the hole-collecting electrode is also of paramount importance for the improvement of the performance of BHJ–PSCs. The summary of performance of conventional PSCs using different anode interlayer designs is listed in Table 3.2 and the chemical structures of organic materials used as anode interlayer in conventional PSCs are shown in Scheme 3.3. In conventional device configuration using ITO as the anode, the polymer complex of poly(3,4-ethylenedioxythiophene):poly(styrene sulfonate) (PEDOT:PSS) has been commonly used as the anode interlayer to improve the contact property between ITO and organic active layer, and to increase the work function of ITO for effective hole collection and transporting [62, 63]. However, it was revealed by Rutherford backscattering (RBS) studies and XPS that the acidic nature of PEDOT:PSS etches the ITO and results in the poor chemical stability at the ITO/PEDOT:PSS interface [64–66]. Moreover, the electrical inhomogeneities of PEDOT:PSS limit its

Table 3.2 Summary of device characteristics of representative conventional PSCs employing different anode interlayers

Anode	Cathode	Active layer	PCE	J_{sc} (mA cm^{-2})	V_{oc} (V)	FF	Ref
ITO/PEDOT:PSS	Al	MEH-PPV:PC$_{61}$BM	0.46	2.1	0.75	0.23	[62]
ITO/PEDOT:PSS/EG	Ca/Al	P3HT:PC$_{61}$BM	4.70	11.5	0.57	0.71	[68]
ITO/MoO$_3$	Ca/Al	P3HT:PC$_{61}$BM	3.33	8.94	0.60	0.62	[70]
ITO/MoO$_3$	TiO$_x$/Al	PCDTBT:PC$_{71}$BM	6.50	10.88	0.89	0.67	[72]
ITO/NiO	LiF/Al	P3HT:PC$_{61}$BM	5.2	11.3	0.64	0.69	[73]
ITO/V$_2$O$_5$	Ca/Al	P3HT:PC$_{61}$BM	3.10	8.83	0.59	0.59	[70]
ITO/WO$_3$	Ca/Al	P3HT:PC$_{61}$BM	3.10	–	–	0.69	[76]
ITO/AgO$_x$	Ca/Al	P3HT:PC$_{61}$BM	4.80	12.70	0.60	0.51	[77]
ITO/TFB:TPDSi$_2$	Al	MDMO-PPV:PC$_{61}$BM	2.23	4.62	0.89	0.54	[78]
ITO/MoO$_3$/TFB	Al	MDMO-PPV:PC$_{61}$BM	2.01	4.28	0.85	0.55	[80]
ITO/SPDPA	Ca/Al	P3HT:PC$_{61}$BM	4.20	10.33	0.60	0.68	[81]
ITO/PTFE	Al	P3HT:PC$_{61}$BM	2.27	7.4	0.52	0.49	[82]
ITO/PEDOT:PSS/P3HT	Ca/Al	P3HT:PC$_{61}$BM	5.05	12.00	0.60	0.69	[85]
FTO/PEDOT:PSS/HAT4	Al	P3HT:PC$_{61}$BM	3.0	9.2	0.57	0.57	[86]
ITO/TPA-PFCB/PEDOT:PSS	Ca/Al	P3HT:PC$_{61}$BM	3.90	9.43	0.61	0.67	[87]
ITO/SWNT/PEDOT:PSS [a]	Al	P3HT:PC$_{61}$BM	4.9	21.0	0.59	0.51	[89]
ITO/PEDOT:PSS/SWNT [a]	Al	P3HT:PC$_{61}$BM	4.9	24.1	0.59	0.44	[89]
ITO/CF$_3$-SAM	LiF/Al	P3HT:PC$_{61}$BM	3.15	13.87	0.60	0.38	[91]

[a] Measured under light intensity of 130 mW cm^{-2}

Scheme 3.3 Chemical structures of organic materials for anode interlayer

electron-blocking ability and thus usually lead to electron leakage at the anode [65, 67]. Therefore, many efforts were devoted to modify PEDOT:PSS in order to achieve the improvement of PSCs performance. Recently, Xiao et al. reported the

enhanced PCE of 4.7 % of P3HT:PC$_{61}$BM solar cell when a layer of ethylene glycol was spin coated over PEDOT:PSS. The enhancement was achieved by the increase of PEDOT:PSS conductivity that improves charge extraction, and enhanced PEDOT:PSS transparency that contributes to enhanced P3HT:PC$_{61}$BM absorption [68]. Soon after, similar work was also reported by Peng et al., who treated PEDOT:PSS layer by ethanol and 2-propanol. Similar enhancement of PCE was also observed when using this treated PEDOT:PSS as anode buffer layer, and this enhancement was attributed to higher conductivity and optimized surface morphology of the PEDOT:PSS [69].

3.2.2.2 Semiconducting Oxides as Anode Interlayer

Aside from the modification of PEDOT:PSS, the development of new materials for hole-collecting/transporting is also vigorously conducted. In principle, an efficient anodic interlayer to substitute PEDOT:PSS should first possess the capability to withstand the organic solvent erosion. Second, a good transparency is desired for the anodic interlayer to guarantee the efficient incident light absorption in organic active layer. Moreover, it should be taken into account as well that the surface properties of the anodic interlayer can significantly influence the phase separation process and morphology of the BHJ active layer.

p-Type semiconducting transition metal oxides such as molybdenum oxide (MoO$_3$), vanadium oxide (V$_2$O$_5$), nickel oxide (NiO), and tungsten oxide (WO$_3$) were hence widely employed as anodic buffer layers to modify the interface between ITO and organic active layer in the conventional BHJ–PSCs. These oxides have relatively large band gap, which guarantee the good optical transparency in visible and near infrared light region of the anode, and consequently allow incident solar photons to reach the organic active layer. More importantly, the Fermi level of these oxides usually positions in the range between 5.0 and 5.4 eV, which align well with the HOMO energy level of most donor conjugated polymers to form ideal Ohmic contact for efficient hole extraction and transporting. Furthermore, the lowest energy level of the conduction band of these *p*-type oxides usually located above 2.5 eV, which is much higher than the LUMO energy level of most organic photovoltaic (OPV) materials (including both acceptors and donors), indicating the good electron-blocking ability of these oxides.

Shrotriya et al. first reported the use of thermally-evaporated MoO$_3$ as the anodic interlayer for BHJ–PSCs to replace PEDOT:PSS [70]. The BHJ–PSCs with 5 nm of MoO$_3$ as anodic interlayer exhibited slightly better performance (3.36 % PCE) than that of PEDOT:PSS device (3.10 % PCE). They revealed as well that an optimized thickness is critical to obtain ideal device performance: a thinner layer of MoO$_3$ results in a smaller V_{oc} and leakage current because of the incomplete coverage, whereas a thicker layer of MoO$_3$ increases the R_s and in turn leads to a smaller J_{sc} and FF [70]. Similar solar cell performance enhancement was also observed by Kim et al. when MoO$_3$ was inserted as anodic buffer layer between ITO and organic active layer [71]. Most recently, Sun et al. reported encouraging

results about the use of thermally-evaporated MoO_3 as the anodic buffer layer of BHJ–PSCs with the configuration of $ITO/MoO_3/PCDTBT:PC_{71}BM/TiO_x/Al$. The implementation of MoO_3 improved the light absorption with the organic active layer, and thereby resulted in a PCE over 6 % at BHJ layer thickness up to 200 nm. A further enhancement in PCE up to 7.2 % was achieved by using an antireflection coating. In addition, BHJ–PSC with MoO_3 as anodic buffer layer demonstrated much better long-term air stability than that of solar cell fabricated with PEDOT:PSS. The PCE remains at approximately 50 % of the original value after the storage in air for 720 h, while the PCE of control PEDOT:PSS device fell to <10 % of the original value after storage in air for 480 h [72].

Deposition of a thin layer of p-type NiO by pulsed laser onto ITO to replace PEDOT:PSS as anodic interlayer led to significant performance enhancement of BHJ–PSC based on P3HT:PCBM blend. A 5–10 nm NiO layer gives rise to the PCE as high as 5.2%, while the PCE of control PEDOT:PSS device is only 2.4 %. The enhancement was initially attributed to the ideal work function of NiO (5.0–5.4 eV) to match well with the HOMO level of P3HT (5.0), and large band gap (ca. 3.6 eV) of NiO to deliver high transparency and sufficient barrier for electron blocking [73]. After that, Irwin et al. via a multifaceted analysis further revealed that NiO grows as smooth, crystalline, and oriented thin films on ITO substrates to form an optically transparent, electrically uniform, and passivated semiconducting anode coating, which prevents anode electron injection and facilitates anode hole injection [74]. However, the pulsed laser deposition of NiO layer is neither scalable nor a cost effective method. Steirer et al. deposited a thin layer of NiO onto ITO by spin coating a diluted nickel metal organic ink followed by thermal annealing at 250 °C. The BHJ–PSCs from this solution-processed NiO exhibited comparable performances with that of PSCs from pulsed laser deposited NiO and PEDOT:PSS [75].

Thermally evaporated thin layers of V_2O_5 and WO_3 were employed as effective buffer layers on ITO to improve the performance of BHJ–PSCs based on $P3HT:PC_{61}BM$ blend. The devices based on both oxides exhibited comparable performances with those of PEDOT:PSS control device. It was suggested that the ideal work function (4.7 eV) and the relatively high-positioning of the lowest energy level of the conduction band (2.4 eV) of V_2O_5 are beneficial for forming efficient hole-collection injection contact with the organic active layer and to provide sufficient barrier for electron leakage at anode [70]. Han et al. revealed that the uniform amorphous film of WO_3 can effectively planarize an originally rough ITO. P3HT films, grown on WO_3 film, have a higher degree of ordering and larger hole mobility than those grown on PEDOT:PSS [76]. An ultra-thin layer of AgO_x generated through plasma oxidized Ag (1 nm) deposited on ITO was found to be able to improve the contact property of ITO/PEDOT:PSS interface. The enhancement of device performance is suggested to the formation of an interface energy step between ITO and PEDOT:PSS that could improve the charge collection efficiency and the overall efficiency of solar cell devices [77].

3.2.2.3 Organic/Polymer Materials as Anode Interlayer

Despite that *p*-type transition metal oxides exhibited outstanding anode interface modification functions, the fabrication of thin films based on these oxides usually involves high-cost thermal evaporation, which limits their application in large-area devices. Organic hole-collecting/transporting materials were thus greatly desired due to their solution processabilities and their facile tunable properties. A cross-linkable blend of poly[9,9-dioctylfluorene-*co*-*N*-[4-(3-methylpropyl)]-diphenyl-amine] (TFB) and 4,4′-bis[(p-trichlorosiylpropylphenyl)phenylamino]biphenyl (TPDSi$_2$) was spin coated onto a ITO substrate to form a robust, optical transparent, homogeneous film after thermal annealing, which can be used as an effective PEDOT:PSS alternative. TFB:TPDSi$_2$ possesses HOMO and LUMO energy levels of -5.3 and -2.3 eV, respectively, which endow the buffer layer good hole-collecting and electron-blocking ability. As a result, BHJ–PSCs of poly(2-methoxyl-5-((3′,7′-dimethyloctyl)oxyl)-1,4-phenylenevinylene) (MDMO-PPV):PCBM with TFB:TPDSi$_2$ anodic buffer layer delivered much better photovoltaic performance and thermal stability than those of PEDOT:PSS control devices [78]. Interestingly, the use of a double interfacial layer of PE-DOT:PSS + TFB:TPDSi$_2$ could decrease the FF of the solar cells, but increase electron blocking to suppress charge leakage and thereby enhance V_{oc} more than using either PEDOT:PPS or TFB:TPDSi$_2$ independently [79]. After that, Subbiah et al. demonstrated that a double interlayer of MoO$_3$/TFB could also improve the photovoltaic performance of the BHJ–PSC with respect to solar cells with a sole PEDOT:PSS or MoO$_3$ anodic buffer layer, due to the enhanced electron blocking and hole collecting from organic active layer to the anode [80].

Li et al. demonstrated the use of a novel self-doped polymer of sulfonated poly(diphenylamine) (SPDPA) as the anodic buffer layer to replace PEDOT:PSS in P3HT:PC$_{61}$BM solar cell. The polar surface of SPDPA film induces the oriented arrangement of P3HT in the active layer during the spin-coating and film-growing processes, which is beneficial for enhancing the hole mobility, producing a better Ohmic contact at the anode junction and thereby gives rise to an enhanced PCE [81]. The implementation of a thin layer of polytetrafluoroethylene (PTFE) between ITO and P3HT:PC$_{61}$BM was found to form an dipole layer at the anode junction, and thereby facilitate the hole extraction. Compared to the PEDOT:PSS control device, solar cells based on PTFE showed obviously enhanced photovoltaic performance. Note that such an insulated PTFE thin layer was deposited by thermally evaporation, and it thereby can be prepared at low substrate temperatures, which is compatible to the flexible polymer substrates for BHJ–PSCs applications [82].

In addition to the modification of PEDOT:PSS or development of PEDOT:PSS alternatives, the implementation of hole selective transporting materials below or above PEDOT:PSS layers is another effective approach to facilitate hole-collecting and electron-blocking at anode junction, and thereby to improve the performance of BHJ–PSCs. It is well-known that there is a vertical composition gradient in organic blend layer with a profile of PC$_{61}$BM- or PC$_{71}$BM-rich blend adjacent to

PEDOT:PSS and conjugated polymer-rich blend near the cathode side, which is possibly detrimental to charge extraction efficiency [83, 84]. Liang et al. hence simply inserted a thin layer of high molecular weight P3HT between PEDOT:PSS and P3HT:PC$_{61}$BM blend layer to increase the electron-blocking ability of PEDOT:PSS. The extra donor/acceptor interfaces adjacent to the bottom of the composite were created as well, leading to an enhanced photoinduced electron transfer efficiency and photocurrent density. Relative to the 3.98 % PCE of the reference device, the extra P3HT inserted PSC delivered PCE of 5.05 % [85]. The insertion of a discotic liquid crystal of hexabutoxytriphenylene (HAT4) at the interface between anodic buffer layers (PEDOT:PSS, MoO$_3$ or NiO) and organic active layer was also found to be an effective method to improve the photovoltaic performance of P3HT:PC$_{61}$BM solar cell. Atomic force microscopy (AFM) measurement indicate that the ordered hexagonal columnar phase formed in HAT4 layer provides a more efficient pass way for hole transporting, and thereby leads to an enhanced J_{sc} and FF [86].

The insertion of an in situ polymerized triphenylamine-containing polyperfluorocyclobutane (TPA-PFCB) thin layer between ITO and PEDOT:PSS was revealed to be an effective approach to block the electron leakage at anode. After the coverage of TPA-PFCB, the surface roughness of ITO was substantially reduced. Compared to the control PEDOT:PSS solar cell, the implementation of the TPA-PFCB layer increases both V_{oc} and J_{sc}, and thereby gives rise to enhanced PCE. The HOMO and LUMO of TPA-PFCB was measured to be −5.2 and −1.7 eV, respectively, which verified its good charge selective hole-transporting and electron-blocking properties. In addition, FET measurement confirmed that electron transporting is completely blocked by implementation of TPA-PFCB between the organic active layer and the Al source and drain electrodes [87].

3.2.2.4 Carbon Nanotubes as Anode Interlayer

Carbon nanotubes (CNTs) possess high electrical conductivity, approximate work function of ~5.0 eV which match well the work function of ITO and HOMO of most donor polymers, and outstanding optical transparency in a broad spectral range from UV to deep infrared region, making CNTs potential hole-collecting materials for BHJ–PSCs [88]. Chaudhary et al. had inserted CNTs at different interfaces (ITO/PEDOT:PSS, PEDOT:PSS/P3HT:PC$_{61}$BM, and P3HT:PC$_{61}$BM/Al) of P3HT:PC$_{61}$BM solar cell, and had found that only CNTs were incorporated into the interfaces of ITO/PEDOT:PSS or PEDOT:PSS/P3HT:PC$_{61}$BM and the solar cells exhibited obvious enhancement in PCE [89]. Most recently, Hatton et al. had demonstrated that the use of partially oxidized CNTs as anodic buffer layer to replace PEDOT:PSS can effectively facilitate the hole extraction. P3HT:PC$_{61}$BM solar cells with this neutral aqueous processed CNTs anodic buffer layer exhibited comparable photovoltaic performance with that of PEDOT:PSS control device [90].

3.2.2.5 Self-Assembled Monolayers as Anode Interlayer

SAMs with different end groups ($-CH_3$, $-NH_2$, $-CF_3$) were also employed to modify the work function of ITO, and thereby to improve the performance of P3HT:PC_{61}BM solar cell. The work function of ITO increased initially from 4.7 to 5.16 eV after the insertion of a $-CF_3$ substituted SAM molecules, affording a much better match with the HOMO of P3HT for efficient hole extraction at anode junction. Moreover, it was found that the surface properties of the inserted SAMs can greatly influence the morphology of the upper organic active layer. Active layer spin coated onto the hydrophobic surface of $-CF_3$ SAM exhibited little undesired phase separation, leading to a high PCE of 3.15 % for the corresponding solar cell [91].

3.3 Interface Engineering for Inverted Solar Cell Devices

The conventional device structure of BHJ–PSCs has some inherent device stability problems. The transparent conducting ITO used as the hole-collecting contact can be etched over time by the acidic PEDOT:PSS hole-transporting layer [64]. The thermo-deposition of low work-function cathode usually requires high vacuum, thus leading to increases in fabrication costs. Moreover, to avoid the exposure of low work-function cathode to air, encapsulation technologies have to be applied which further complicate the fabrication process. Therefore, device architectures that can remove the need of PEDOT:PSS (or at least separate it from ITO) and use nonvacuum-deposited air-stable high work-function metal electrodes at the top interface are desired. Based on these considerations, inverted solar cell device architecture was proposed. The device structure is shown in Fig. 3.1. This architecture has recently attracted considerable attention due to the device stability and processing advantages compared to the conventional architecture. In an inverted device, the polarity of charge collection is the opposite of the conventional architecture, allowing the use of higher work function and air-stable materials (Au, Ag, and Cu) as the top anode which is exposed to air. The use of higher work-function metals offer better ambient device stability and the possibility for using low-cost solution-processed techniques such as spray coating [92] or screen printing [93] to deposit the top anode. The focus of current research for the inverted device architectures is to understand how to improve the device efficiency and stability through the design and processing of the different interfacial layers in the device structure. In this section, we will review the recent progress of interface engineering for inverted solar cells in two aspects: the progress in anode interlayer design and the progress in cathode interlayer design.

3.3.1 Cathode Interlayer

In principle, ITO is capable of collecting either electrons or holes since its work function (4.5–4.7 eV) lies between the typical HOMOs and LUMOs of common OPV materials. Therefore, the polarity of ITO can be modified to efficiently collect either electrons or holes by coating functional interlayers of different work functions onto its surface [29]. For inverted solar cell application, electron transporting layers (ETL, or electron selective layer) with low work function are formed on top of ITO to modify the ITO interface for efficient electron extraction and collection from active layer. Such ETL materials typically include inorganic ones like Cs_2CO_3 [29, 33], Ca [94], Al_2O_3 [95], ZnO [96–98], and TiO_x [99, 100]. Since light needs to pass through the ETL to reach the active layer to generate photocurrent, the layers are typically very thin to maintain high optical transmittance. The electron mobility and work function of the ETL layer should also be optimized in order to realize efficient electron collection. The summary of performance of inverted PSCs using different ETL designs is listed in Table 3.3 and the chemical structures of organic materials used as ETL in inverted PSCs are shown in Scheme 3.4 (WPF-6-oxy-F is shown in Scheme 3.2).

3.3.1.1 Metal Oxide Thin Film as ETL

ZnO and TiO_x are the most commonly utilized ETL materials for inverted solar cells due to the high optical transparency in the visible and near infrared region, high carrier mobility, and its solution processibility. Many demonstrations of using these *n*-type metal oxide layers as the electron selective layer for inverted solar cells have been reported in literatures.

An efficient P3HT:PC_{61}BM BHJ inverted solar cell from a high-temperature processed sol–gel ZnO interlayer on ITO and an Ag electrode as the top hole-collecting contact was first demonstrated by White et al. [96]. The zinc acetate (ZnAc) sol–gel precursor was directly spin cast onto ITO and then thermally annealed at 300 °C for 5 min to hydrolyze and crystallize into amorphous ZnO thin film. Improved conductivity and mobility after annealing led to conversion efficiencies of 2.97 % of the inverted device. Interestingly, it was found that when these devices were exposed to air, the performance gradually improved. They attribute the improvement to the oxidation of Ag which formed Ohmic contact with P3HT. State-of-the-art inverted solar cell using ZnO as ETL and a low-bandgap donor material PCDTBT can yield PCE as high as 6.33 % [97]. To further improve the electronic properties of ZnO, Al doping was explored and inverted devices with Al-doped ZnO (AZO) as ETL were thus fabricated [101, 102]. Although the AZO device performance is not greatly improved compared to undoped ZnO devices, AZO layer can be made much thicker (>100 nm) than ZnO layer without hampering the solar cell performance; thus, it is more robust and easier to process.

Table 3.3 Summary of performances of inverted polymer solar cell devices using different ETL designs

ETL	Active Layer	Anode	PCE (%)	J_{sc} (mA cm^{-2})	V_{oc} (V)	FF (%)	Ref
Cs_2CO_3	P3HT:PC$_{61}$BM	V$_2$O$_5$/Al	2.25	8.4	0.56	62.1	[29]
Cs_2CO_3 [a]	P3HT:PC$_{61}$BM	V$_2$O$_5$/Al	2.10	8.8	0.55	56.3	[29]
Ca	P3HT:PC$_{61}$BM	MoO$_3$/Ag	3.55	8.3	0.65	65.9	[94]
Al$_2$O$_3$	P3HT:PC$_{61}$BM	PEDOT:PSS/ Ag	2.82	7.7	0.57	64.0	[95]
ZnO	P3HT:PC$_{61}$BM	Ag	2.97	11.2	0.56	47.5	[96]
ZnO	PCDTBT:PC$_{71}$BM	MoO$_3$/Al	6.33	10.4	0.88	68.8	[97]
ZnO	PSiFDBT:PC$_{61}$BM	Au	3.80	5.03	0.90	60.0	[98]
TiO$_x$	P3HT;PC$_{61}$BM	PEDOT:PSS/ Au	3.10	9.0	0.56	62.0	[99]
PTE/TiO$_x$	P3HT:PC$_{61}$BM	PEDOT:PSS/ Ag	3.5	10.5	0.55	60.0	[100]
AZO [b]	P3HT:PC$_{61}$BM	PEDOT:PSS/ Ag	2.59	9.6	0.57	47.7	[101]
ZnO NP [c]	P3HT:PC$_{61}$BM	PEDOT:PSS/ Ag	3.61	10.7	0.62	54.2	[103]
ZnO NP/C$_{60}$SAM	P3HT:PC$_{61}$BM	PEDOT:PSS/ Ag	4.54	12.0	0.63	60.6	[105]
TiO$_x$/C$_{60}$SAM	P3HT:PC$_{61}$BM	PEDOT:PSS/ Ag	3.80	10.6	0.62	57.2	[110]
TiO$_x$/FPQ-Br	P3HT:PC$_{61}$BM	MoO$_3$/Au	3.55	8.9	0.58	70.0	[111]
ZnO/PCBSD	P3HT:PC$_{61}$BM	PEDOT:PSS/ Ag	4.40	12.8	0.60	58.0	[112]
ZnO/PCBSD	P3HT:ICBA	PEDOT:PSS/ Ag	6.22	12.4	0.84	60.0	[113]
PEO	APFO:PC$_{61}$BM	PEDOT-EL/ PH500	0.70	2.3	0.67	45.0	[114]
WPF-6-oxy-F	P3HT:PC$_{61}$BM	PEDOT:PSS/ Ag	3.38	8.8	0.66	59.0	[115]
WPF-6-oxy-F [d]	P3HT:PC$_{61}$BM	PEDOT:PSS/ Ag	1.23	6.6	0.57	33.0	[116]
P3PHT$^+$/(PEDOT: PSS)$^-$	P3HT:PC$_{61}$BM	V$_2$O$_5$/Al	1.85	7.1	0.54	46.0	[117]
DCM doped PCBM-S	P3HT:PC$_{61}$BM	PEDOT: PSS/ Ag	2.53	9.1	0.64	44.0	[118]
no ETL	P3HT:PC$_{61}$BM	PEDOT:PSS/ Ag	4.10	11.7	0.62	57.0	[119]

[a] Solution processed
[b] Nanoparticles
[c] Aluminum doped ZnO
[d] On graphene substrate

TiO$_x$ sol–gel layer ($\sim$10 nm) was also demonstrated as an effective ETL for inverted solar cells [99]. The devices with structure of ITO/TiO$_x$/P3HT:PC$_{61}$BM/PEDOT:PSS/Au showed a PCE of 3.1 %. O-xylene was used as solvent for
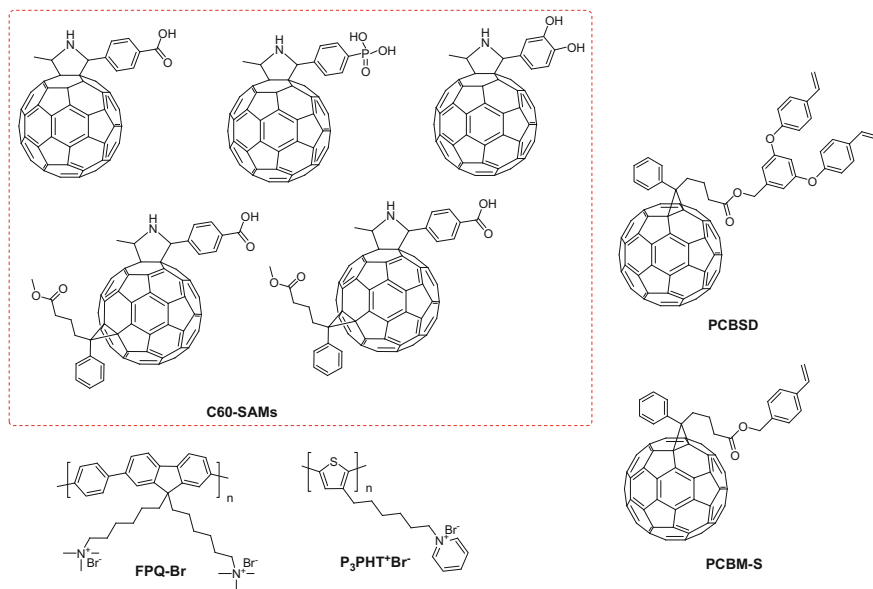
Scheme 3.4 Chemical structures of organic materials used in ETL for inverted polymer solar cells

P3HT:PC$_{61}$BM instead of the commonly used chlorobenzene or dichlorobenzene to make the vertical phase segregation of donor and acceptor more favorable for inverted devices. Like in the case of conventional devices, controlling the bulk blend vertical phase segregation is also important in inverted devices; however, the optimal phase segregation is different from the case of conventional devices [84].

3.3.1.2 Metal Oxide Nanoparticle Layer

One of the problems of sol–gel process of ZnO and TiO$_x$ is that they require high temperature annealing processing conditions in order to improve the crystallinity of the material to minimize resistive losses in the solar cell devices. These high temperature processing conditions can reach as high as 500 °C, which is not compatible with industry scale roll-to-roll process. To overcome this problem, ZnO NPs are introduced as ETL materials for inverted solar cells [41, 103]. The devices fabricated from the ZnO NPs on ITO-coated glass show an average PCE of ∼3.6 %. This value is very similar to that obtained from the high temperature processed ZnO sol–gel devices on glass/ITO which show an average efficiency of ∼3.5 %. This demonstrates that sol–gel ZnO and ZnO NPs thin film layers can both act as a good electron selective layer in the inverted device architecture.

3.3.1.3 Self-Assembled Monolayer on Metal Oxide Surface

Although reasonable efficiencies have been reached with n-type metal oxides as the electron selective layer in inverted solar, it still has great room for improvement, as the surface of metal oxides have hydroxyl groups that can cause charge trapping at the metal oxide/active layer interface [104]. These hydroxyl groups terminated surfaces lead to high-interface charge recombination due to poor charge transfer. One approach that can improve the electrical and morphological properties of metal oxide/active layer interface is to utilize a SAM between the inorganic and organic interface [40, 91, 105–109]. SAMs can be utilized to significantly modify the interfaces of oxide and metallic surfaces to improve adhesion, compatibility, charge-transfer properties, energy level alignment, and affect the upper layer growth of materials. It was demonstrated that modifying the metal oxide surfaces of TiO_2 and ZnO-based inverted solar cells with a fullerene-based SAM (C_{60}-SAM) can improve the device performance. The C_{60}-SAM affects the photo-induced charge transfer at the interface to reduce the recombination of charges, passivate inorganic surface trap states, improve the exciton dissociation efficiency at the polymer/metal oxide interface as well as act as a template to influence the overlayer BHJ distribution of phases and crystallinity leading to higher efficiency inverted solar cells [105, 110].

3.3.1.4 Polymer and Cross-Linked Interlayer on Metal Oxide Surface

The potential drawbacks for SAM formation on metal oxide surface are incomplete coverage at the molecular scale and probable desorption of this monolayer during wet processing, creating localized defects in this interlayer [109]. The other approach that can improve the metal oxide/active layer interface is to insert an organic ETL interlayer in between. In order to resist the solvent washing from the over-layer, this organic layer should have orthogonal solubility with active layer, or it should be cross-linkable. Choi et al. reported a remarkable improvement in inverted solar cell performance by employing a thin layer of CPE on top of TiO_x. The TiO_x/CPE composite ETL improves the electron injection and transport at the cathode and blocks the hole transport to the cathode, leading to a PCE improvement from 2.65 to 3.55 % [111]. The CPE material was alcohol soluble, and thus not affected by the solvent of the active layer. Hsieh et al. reported a $PC_{61}BM$-based n-type material [6,6]-phenyl-C_{61}-butyric styryl dendron ester (PCBSD) functionalized with a dendron containing two styryl groups as thermal cross-linkers [112]. By heating at 160 °C for 30 min a robust, adhesive, and solvent-resistant thin film can be generated on top of ZnO layer. An inverted solar cell device based on ITO/ZnO/cross-linked PCBSD/P3HT:$PC_{61}BM$/PEDOT:PSS/Ag configuration not only achieves enhanced device characteristics (PCE 4.4 %), but also exhibits an exceptional device lifetime without encapsulation; it greatly outperforms a reference device (PCE 3.5 %) based on an ITO/ZnO/P3HT:$PC_{61}BM$/PEDOT:PSS/Ag configuration without the interlayer. Changing the acceptor in the active layer from $PC_{61}BM$ to a novel fullerene derivative indene-C_{60} bis-adduct (ICBA) can further

improve the PCE of inverted solar cell device with PCBSD interlayer [113], yielding a record efficiency of 6.2 % for inverted organic solar cell devices at the time.

3.3.1.5 Polymer or Cross-linkable Organic Thin Film as Single ETL

Besides acting as an interlayer between metal oxide layer and active layer, polymer or cross-linkable organic thin films can also be implemented as independent ETL for inverted solar cells to completely replace the metal oxide layer. Zhou et al. reported the use of PEO thin film as single ETL on ITO for inverted solar cells. The insertion of PEO interlayer between ITO and APFO3:$PC_{61}BM$ active layer improved the PCE of the devices from 0.5 % to 0.7 % [114]. Na et al. later reported the use of a water-soluble polyfluorene CPE as a single ETL which can improve the PCE of P3HT:$PC_{61}BM$ inverted devices from 1.04 % without interlayer to 3.38 % [115]. The same group found out that the CPE material can also be an effective ETL for multilayered graphene (MLG) cathode [116]. An inverted solar cell device with configuration of MLG/CPE/P3HT:$PC_{61}BM$/PE-DOT:PSS/Al has a PCE of 1.23 %, while the reference device without CPE interlayer has virtually no photovoltaic effect at all. In these studies, the increase in PCE is explained by the enhancement of built-in voltage due to work function lowering effect of the interlayer, and this is generally supported by work function measurement of ITO substrate with or without interlayer through ultraviolet photoelectron spectroscopy (UPS) or Kelvin probe.

Besides common solution process, polymer ETL can also be fabricated by layer-by-layer (LBL) method. Rider et al. reported an ETL generated by repeated LBL deposition of cationic water-soluble polythiophene poly[3-(6-pyridiniumylhexyl) thiophene bromide] (P3PHT$^+$Br$^-$) with anionic (PEDOT:PSS)$^-$Na$^+$ on ITO [117]. The inverted solar cell device of ITO/(P3PHT$^+$/(PEDOT: PSS)$^-$)$_5$/P3HT:$PC_{61}BM$/ V_2O_5/Al has an efficiency of ~ 2 % and operation lifetime >500 hours.

As the organic ETL materials generally suffer from their low electron conductivity compared to metal oxides, some researchers try to compensate this by doping the ETL layer. Cho et al. demonstrated that the n-doping of a cross-linkable $PC_{61}BM$ derivative PCBM-S using decamethylcobaltocene (DMC) can significantly increase the electron conductivity of the cross-linked ETL layer [118]. In the configuration of ITO/PCBM-S/P3HT:$PC_{61}BM$/PEDOT:PSS/Ag, device with PCBM-S layer of optimum DMC doping level yield a PCE of 2.53 %, compared to 1.24 % for devices with undoped PCBM-S interlayer.

Before the end of this section it should be noted that the electronic properties of the interface of ITO and metal oxide is complicated and our understanding is far from complete. For example, Wang et al. reported an interesting case that the PCE of the inverted solar cell device with the structure of ITO/P3HT:$PC_{61}BM$/PE-DOT:PSS/Ag changes irreversibly from 1.46 to 4.1 % when the device is exposed to continuous illumination of simulated sunlight for 2 h [119]. Though the mechanisms behind the large enhancement in PCE is not thoroughly explained, the

fact that high PCE can be achieved in a device without ETL poses the question of how and to what extent an ETL can improve the electron-collecting ability of ITO in inverted devices.

3.3.2 Anode Interlayer

Direct contact of the top high work-function metal to the active layer can lead to degradation of the solar cell performance, therefore, a hole-transporting/electron-blocking layer (HTL/EBL) is generally deposited between these two layers to improve charge selectivity and collection of holes. The materials that have been utilized as HTL are various high work-function transition metal oxides such as MoO_3, or denoted as MoO_x because of oxygen vacancy formed during thermo-evaporation [97, 120, 121], WO_3 [122, 123] and V_2O_5 [29, 124], and solution-processed organic materials including PEDOT:PSS [99, 112, 113], SPDPA [125], dextran-doped poly(allylamine hydrochloride) (PAH-D) [126], and cross-linkable molecule N,N′-diphenyl-N,N′-bis-(3-methylphenyl)-(1,1′)-biphenyl -4,4′- dia-mine- bis (vinyl benzyl ether) (TPD-BVB) [127]. The chemical structures of the organic HTL materials are shown in Scheme 3.5 (PEDOT:PSS and SPDPA are shown in Scheme 3.3).

3.3.2.1 PEDOT:PSS as HTL or Anode

The literature on HTL design of inverted solar cells is relatively scarce compared to ETL. For solution-processed HTL PEDOT: PSS is often used. The challenge of using PEDOT:PSS as HTL in an inverted device is that PEDOT:PSS is an aqueous dispersion and it is difficult to coat it onto an organic active layer due to its hydrophobic property. Cosolvent [99] or surfactants [112] are added to improve interfacial compatibility of PEDOT: PSS and active layer. However, the conformation of PEDOT:PSS using these methods was different and consequently its work function and conductivity would be changed. Another way to uniformly
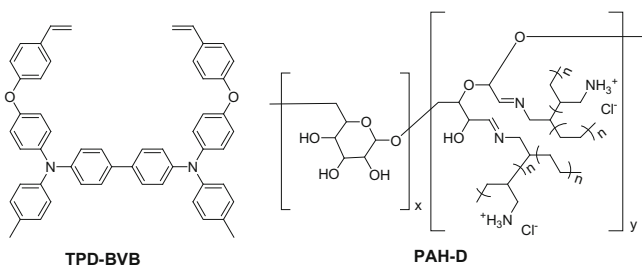
Scheme 3.5 Chemical structures of organic HTL materials for inverted polymer solar cells
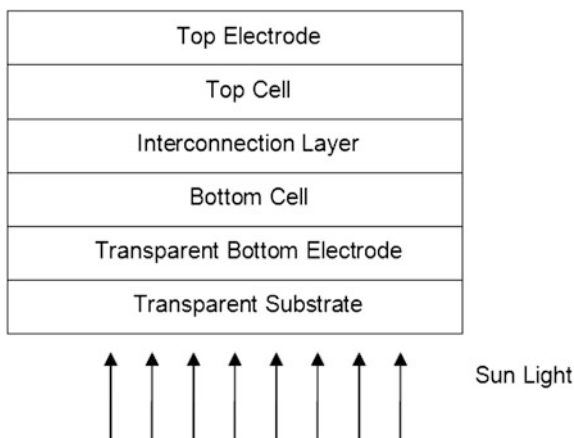
deposit PEDOT:PSS onto an active layer is to use spray coating technique [128]. By incorporating D-sorbitol into PEDOT:PSS, a transparent "electric glue" can be formed, which is capable of laminating films together both mechanically and electrically [129]. Implementing the unique property of the "electric glue" into the inverted device, a semitransparent polymer solar cell based on the $P3HT:PC_{61}BM$ blend was fabricated by the lamination process with a 3 % PCE [130]. This method took advantage of the solution process, which also featured self-encapsulation and provided an alternative to the roll-to-roll production of inverted solar cells.

PEDOT:PSS in its high conductivity form can be directly used as anode for inverted solar cells. Lim et al. spray coated a layer of modified PH500 (300 S cm^{-1}) high conductivity PEDOT:PSS onto $ITO/Cs_2CO_3/P3HT:PC_{61}BM$ to form the anode, and the PCE of the device was 2 % [63]. Though the conductivity of PEDOT:PSS layer formed by spray coating was not optimized compared to spin-coating method, the advantage of spray deposition is that very thick films can be obtained, which makes up for the low conductivity. Zhou et al. went one step further to use PH1000 (900 S cm^{-1}) high conductivity PEDOT:PSS as both anode and cathode for semitransparent inverted solar cells [131]. The device structure was $PH1000/ZnO/P3HT:PC_{61}BM/CPP$-PEDOT (a low conductivity PEDOT: PSS)/PH1000, and the PCE was 1.8 %.

3.3.2.2 Solution Processable Metal Oxide HTL

Though the best inverted solar cells are fabricated with thermo-evaporated transitional metal oxide HTL such as MoO_3 or V_2O_5, solution processable HTL is preferred since vacuum evaporation could detract from the advantage of the ease of polymer solar cell fabrication. Therefore, some efforts are made to design solution-processing route for transitional metal oxide materials. Huang et al. dispersed V_2O_5 powder in isopropanol through ultrasonic agitation and spin cast the dispersion onto $P3HT: PC_{61}BM$ active layer to form HTL [124]. The device with configuration ITO/ZnO nanorod/$P3HT:PC_{61}BM/V_2O_5/Ag$ has a PCE of 3.56 % under optimum V_2O_5 thickness, compared to 2.24 % for reference device without the V_2O_5 layer. Later, it was found that NiO NPs can also be dispersed in isopropanol and spin cast onto active layer to form HTL. Lim et al. reported solution-processed NiO as single HTL [132] and Lin et al. reported the solution process of NiO/plexcore HTL double layer HTL [133]. A sol–gel solution process of copper (I) oxide (Cu_2O) HTL similar to the sol–gel process of ZnO was recently reported [134]. Deionized water was added into the copper (II) acetate monohydrate precursor solution to trigger sol–gel reaction and the solution is then spin cast onto active layer to form Cu_2O layer in situ. PCE of the devices with the Cu_2O HTL are improved from 3.34 to 4.02 %.

Fig. 3.2 Schematics of common double junction tandem solar cell device structure

| Top Electrode |
| Top Cell |
| Interconnection Layer |
| Bottom Cell |
| Transparent Bottom Electrode |
| Transparent Substrate |

↑ ↑ ↑ ↑ ↑ ↑ ↑   Sun Light

3.4 Interface Engineering for Organic Tandem Solar Cell Devices

To improve the absorption of the sunlight photons by organic solar cells, active materials with a broader absorption spectrum have to be designed. This is generally achieved by reducing the band gap of the material which could lead to lower V_{OC} in the devices. Another strategy is to apply tandem device structure in which multiple absorbers with different band gaps are to be stacked or mixed in multiple junctions. When two or more donor materials with nonoverlapping absorption spectra are used in a tandem solar cell, broader range of the solar spectrum can be covered without sacrificing V_{OC} of the device, as the thermalization of hot carriers can be minimized [135]. The most commonly employed tandem cell structure is a two terminal monolithic device in which two subcells are connected in series through an interconnecting layer (ICL), as shown in Fig. 3.2. Several approaches for organic tandem cells have been reported in recent years, depending on the materials used for the active layer and the respective interconnection layers. In general, the organic tandem solar cells can be divided into three classes [136]: (1) Tandem organic solar cells in which low-molecular-weight molecules are used for both the bottom and the top cells; (2) Hybrid tandem organic solar cells in which the bottom cell is processed from polymers by solution-processing, while the top cell is made of vacuum-deposited low-molecular-weight molecules; (3) Fully solution-processed tandem organic solar cells in which both the bottom and the top cells are BHJ–PSCs. The third class of organic tandem solar cells began to receive enormous attentions since Kim et al. successfully fabricated an all solution-processed (except the cathode) tandem cell device with a record efficiency of 6.5 % in 2007 [12]. The interface problems in such tandem solar cell devices are much more complicated than single junction devices, as more layers are incorporated into a single device.

The ICL, both physically and electrically, connects the two subcells in an organic tandem solar cell device and it is critical in the fabrication of highly

Table 3.4 Summary of performances of organic tandem solar cell devices using different ICL designs

ICL	Bottom Cell	Top Cell	PCE (%)	J_{sc} (mA cm^{-2})	V_{oc} (V)	FF (%)	Ref
Au	H$_2$PC/Me-PTC	H$_2$PC/Me-PTC	∼1	–	0.78	–	[137]
Ag	CuPc/PTCBI	CuPc/PTCBI	2.30	6.5	0.93	38.0	[138]
Au	P3HT/PC$_{61}$BM [a]	ZnPc:C$_{60}$	2.30	4.8	1.02	45.0	[139]
n-doped C$_{60}$/Au/p-doped MeO-TPD	ZnPc:C$_{60}$	ZnPc:C$_{60}$	3.80	12.0 [b]	0.99	47.0	[140]
BPhen:Li/Au/ MTDATA:F4-TCNQ	P3HT:PC$_{61}$BM	CuPc/C$_{60}$	1.20	2.5	0.99	47.0	[141]
Al/WO$_3$	P3HT:PC$_{61}$BM	CuPc:C$_{60}$	4.60 [c]	–	–	–	[142]
LiF/Al/MoO$_3$	P3HT:PC$_{61}$BM	CuPc:C$_{60}$	2.82	6.1	1.01	46.2	[143]
ITO/PEDOT:PSS	MDMO-PPV:PC$_{61}$BM	MDMO-PPV:PC$_{61}$BM	3.10	4.1	1.34	56.4	[144]
LiF/Al/Au/PEDOT:PSS	PFDTBT/PC$_{61}$BM	PTBEHT/PC$_{61}$BM	1.40	0.9	55	57.0	[145]
ZnO/neutral PEDOT	MDMO-PPV:PC$_{61}$BM	P3HT:PC$_{61}$BM	1.90	3.0	1.53	42.0	[146]
TiO$_2$/Al/PEDOT:PSS	P3HT:PC$_{71}$BM	PSBDTBT:PC$_{71}$BM	5.84	7.4	1.25	63.2	[147]
TiO$_x$/PEDOT:PSS	PCPDTBT:PC$_{61}$BM	P3HT:PC$_{71}$BM	6.50	7.8	1.24	67.0	[12]
MoO$_3$/Al/ZnO(Inverted)	P3HT:PC$_{61}$BM	PSBDTBT:PC$_{71}$BM	5.10	7.8	1.20	54.1	[149]
MoO$_3$/Ag/Al/Ca (Inverted)	P3HT:PC$_{61}$BM	P3HT:PC$_{61}$BM	2.78	3.81	1.18	61.8	[150]

efficient tandem devices. Inappropriate design of the ICL could lead to electrical or optical losses which would in turn result in the loss of performance, and most notably the loss of V_{OC}. The role of the ICL in tandem devices is threefold: (1) it should efficiently collect electrons from one subcell and holes from another subcell; (2) it should act as an efficient recombination zone so that charge accumulation in this layer is minimized; (3) for all solution-processed tandem devices, it should also act as effective separation layer to protect the bottom cell from dissolving during processing of the top cell.

In this section, we focus on the design and fabrication of ICLs in organic tandem solar cells since the most important interfacial engineering problems are related to this layer. The summary of organic tandem solar cell performance using different ICL designs is listed in Table 3.4.

3.4.1 Thermally Evaporated ICL

In small molecule tandem cells, the acceptor layer of bottom cell and the donor layer of the top cell can be completely separated to prevent formation of an inverse p–n junction by the simple incorporation of an ultra-thin layer of Au [137] or Ag [138]. However, if a thin layer of metal is used as ICL in a tandem cell with at least one polymer BHJ as subcell, the interlayer contacts both the acceptor and donor domains of the BHJ, making the selective extraction of electrons or holes from the polymer BHJ impossible. To overcome this problem, diffused bilayer polymer

heterojunction can be used instead of a BHJ, so that only $PC_{61}BM$ contacts the metal layer [139]. Another approach is to have additional hole-blocking or electron-blocking layers in the ICL. Heavily doped p–n junction as ICL was proposed to ensure Ohmic contact between the subcells [140, 141]. This approach allowed the addition of the V_{OC} of individual subcells in tandem architectures with minimal loss due to absorption or reflection in the interlayer. More importantly, the good electrical contact of the ICL does not depend on the choice of photoactive materials.

More commonly used ICL design for tandem cells is the bilayer composite consisting of a low work-function (*n*-type) layer and a high work-function (*p*-type) layer [142]. Typical materials used for *p*-type layer are high work-function metal oxides such as MoO_3 or WO_3. These metal oxides can easily form Ohmic contact with organic active layers and they are also highly transparent. Zhao et al. used MoO_3 as high work-function contact for the top cell and a bilayer of LiF and Al forming a low work-function contact with the bottom cell [143]. Negligible optical loss in the ICL was observed because of almost 100 % transmittance of the interlayer and no potential losses were observed either.

A major challenge in fabricating polymer tandem cells is the processing of the top cell without damaging the underlying layers. Thus, the criterion for choosing the materials for ICL, besides Ohmic contact forming ability, is the robustness of the thin film so that it can withstand any solution process and protect the bottom cell layers. Kawano et al. demonstrated a polymer tandem cell using ITO/PEDOT:PSS as ICL [144]. The ITO layer in the ICL was sputtered onto bottom cell active layer in 1 Pa of argon gas so that the damage in active layer can be prevented during sputtering. It was found that 20 nm of ITO was sufficient to protect the underlying active layer from solution process of the top cell. Hadipour et al. used an efficient multilayer ICL consisting of *n*-type and *p*-type layers [145]. The *n*-type layers were LiF/Al and the *p*-type layers were Au/PEDOT:PSS. Au layer was deposited to protect the bottom LiF/Al contact from the solution process of the top cell. V_{OC} of the tandem cell was equal to the sum of V_{OC} of the component cells which shows the effectiveness of the ICL. However, the disadvantage of using metal layers is the loss of incident photons for the top cell.

3.4.2 Solution-Processed ICL

The real advantage of polymer solar cells is the ease of fabrication using solution process, thus the development of solution-processed ICL for tandem cells is necessary in order not to compromise this advantage. There were many reports on solution-processed electron transport layers such as ZnO and TiO_2 (or TiO_x), that can be used as *n*-type layers in the ICL. These electron transport layers are wide-band-gap semiconductors and are highly transparent to sunlight. PEDOT:PSS, being a high work-function conducting polymer, is predominantly used to form Ohmic contact for holes with the polymer BHJ and is an alternative to thermally

evaporated high work-function metal oxides. The first demonstration of all solution-processed polymer tandem cells was using ZnO NPs dissolved in acetone to deposit the *n*-type layer, and aqueous-based neutral pH PEDOT:PSS as the *p*-type layer [146]. ZnO has been shown to form an efficient contact for electron extraction from polymer BHJ because of its matching energy level with $PC_{61}BM$. The alcohol dispersed ZnO NPs does not damage the bottom polymer layer and aqueous-based neutral PEDOT:PSS layer does not affect the ZnO layer. Such an ICL is robust enough to protect the bottom polymer cell from any subsequent solution process. It was thus guaranteed that during the entire fabrication process, none of the solution process steps damaged the previously formed layers. Using these solution-processed ICLs, double and triple junction tandem cells were shown with only minor losses in V_{OC}.

Sol–gel derived TiO_2 is another potential candidate as an *n*-type contact. Kim et al. and Sista et al. used sol–gel based TiO_2 layer for efficient electron extraction from the bottom cell and PEDOT:PSS as a *p*-type layer [12, 147]. Though the synthesis approaches of TiO_2 employed by the two groups are totally different, highly efficient tandem cells were both demonstrated without V_{OC} losses. Kim et al. used a TiO_x precursor solution to coat 20–30 nm thick dense films on polymer layer that was followed by baking in air for hydrolysis of precursor into solid state TiO_x. The purpose of the TiO_x layer was threefold: being an electron transport layer, a hole-blocking layer, and an optical spacer. On the other hand, Sista et al. used crystalline NPs of TiO_2 dispersed in alcohol solvent to form an electron transport layer [148]. Several other reports on solution-processed tandem cells have used ZnO or TiO_2 via various processes as *n*-type contact and PEDOT:PSS for *p*-type contact, yielding efficient tandem cells.

3.4.3 Efficient Recombination Inside ICL

The charge recombination rate inside the ICL should match the charge extraction rate from the two sub cells, otherwise it will lead to accumulation of charges in the ICL, increasing the R_s and even induces significant loss in the photocurrent near V_{OC}, resulting in low efficiency devices with S-shaped *J*–*V* curves.

Gilot et al. observed such S-shaped *J*–*V* curves in their tandem solar cell devices and they attributed the problem to the non-Ohmic contact between ZnO and PEDOT:PSS in the ICL, which would form a counterdiode, and thus hinders charge recombination [146]. To restore efficient charge recombination in the ICL, a thin Ag layer was inserted between ZnO and PEDOT layer, and the S-shaped curve disappeared. Alternatively, an Ohmic contact between *n*-type and *p*-type layers inside ICL can be formed by heavily doping the two layers. In the case of PEDOT:PSS/ZnO ICL, further doping of PEDOT:PSS is not necessary, and the doping level of ZnO was increased by UV irradiation. Gilot et al. observed that the S-shaped curve disappears soon after UV irradiation and the V_{OC} of the tandem cell increases. Similar cases were reported by Sista et al. in tandem solar cell

devices using PEDOT:PSS/TiO$_2$ ICL [147]. They observed S-shaped curves in such tandem devices, and when the devices were irradiated with UV light of wavelength below 400 nm, the *J–V* characteristics returned to normal and the PCE was thus greatly improved.

The UV activation phenomenon described above is useful to study the interface interaction between transitional metal oxides and heavily-doped conjugated polymers. A similar behavior was observed for single junction devices with TiO$_2$/ PEDOT:PSS/Al as the composite cathode, confirming the theory that this transition from a high resistance state to a low resistance state is the result of Schottky-to-Ohmic transition of PEDOT:PSS/TiO$_2$ contact [147]. The *p*-type PEDOT:PSS and *n*-type TiO$_2$ form a metal–semiconductor contact with a triangular barrier at the TiO$_2$/PEDOT:PSS interface. At a low doping level of TiO$_2$, the triangular barrier width is large and blocks electrons in TiO$_2$ to recombine with holes from PEDOT:PSS. After irradiating with UV light, the free carrier concentration in TiO$_2$ increases significantly and the barrier width decreases to an extent that electrons can tunnel through the barrier. However, this transition to Ohmic contact is not permanent, as the device reverts back to the high resistance state after prolonged storage in the dark. Thus, methods that can realize stable doping of metal oxides are desired. One approach is the chemical doping using electron-donating species. Park et al. reported the doping of TiO$_2$ NPs by Cs$_2$CO$_3$ [148], causing a significant energy level shift of TiO$_2$. It was observed that Ti ions were partially reduced by Cs ion through charge transfer, thus increasing the *n*-type doping.

3.4.4 ICL for Inverted Tandem Solar Cells

As reported by Chou et al., the advantages of the tandem and inverted structure can be combined by employing a metal oxide-only interlayer (MoO$_3$/Al/ZnO) to connect two inverted BHJs devices [149]. An inverted tandem solar cell with P3HT:PC$_{61}$BM and poly[(4,4′-bis(2-ethylhexyl)dithieno[3,2-b:2′,3′-d] silole)-2,6-diyl-alt-(2,1,3-benzothiadiazole)-4,7-diyl] (PSBTBT, see Scheme 3.1):PC$_{71}$BM as bottom cell and top cell respectively can reach a PCE of 5.1 %. A low temperature hydrolysis process was developed to form a dense and smooth amorphous ZnO layer with excellent diode properties, while the crystalline ZnO appears rougher and more porous. In addition, the MoO$_3$ provides a much robust resilience against the sol–gel process compared to V$_2$O$_5$ or Al. As a result, the materials and configurations of the interlayer for the tandem architecture were no longer limited by the acidic PEDOT:PSS. Compared to PEDOT:PSS, the absorption of the metal oxide-based interlayer is also smaller, resulting in higher photocurrent for both single and tandem cells. Sun et al. also reported a multilayered ICL in inverted tandem cells [150]. MoO$_3$/Ag/Al/Ca interlayer was vacuum deposited, and followed by deposition of the rear cell via spin-coating process. Such an interlayer structure features high transparency and low R_s, as well as effective charge

recombination, rendering an exact summation of V_{oc} (1.18 V) of the two subcells and a high FF (61.8 %). Maximum PCE of 2.78 % is mainly due to the fact of using identical subcells.

3.5 Summary and Outlook

The overall performance of BHJ–PSCs (for either conventional device, inverted device, or tandem device) is determined by a series of sequential optoelectronic processes including charge separation, transporting, and extraction, which can be controlled by the manipulation of intrinsic properties of the photoactive materials, the morphology of active layer and the electrical contact of interfaces between different layers, etc. The interface problems between different thin film layers inside a polymer solar cell device is neglected for a long time by researchers as most of their efforts were devoted to the development of new active materials, the optimization of active layer morphology. Thus only until recently did the main-stream researchers realize the importance of interface engineering on the photo-voltaic performance of devices. Great improvements in performance were thus achieved for BHJ–PSCs field via the understanding of interface function and the development of highly efficient interface modification materials. As discussed in this chapter, the interlayers function in many aspects, such as improving interfacial electrical contact, passivating charge trapping states, altering electrode work function, controlling energy alignment, enhancing charge collection, inducing active layer phase separation, redistributing the incident light field, and even improving the yield and quality of device fabrication process. However, most of the reported interfacial materials function only the above-mentioned aspects par-tially and may result in some side effects. Moreover, some interfacial materials are sensitive to the active layer, i.e., functional for some certain photovoltaic materials but not for others. Therefore, the integration of all kinds of different functions into one material is still challenging and in the near future, the development of more efficient interfacial materials is still required. Nevertheless, the great progress in the field of BHJ–PSCs gives the researchers opportunity and confidence to develop more powerful interfacial materials and roll-to-roll compatible fabrication meth-ods, and thereby pave the way for commercialization of polymer solar cells.

References

1. Günes S, Neugebauer H, Sariciftci NS (2007) Conjugated polymer-based organic solar cells. Chem Rev 107:1324–1338
2. Thompson BC, Fréchet JMJ (2008) Polymer–fullerene composite solar cells. Angew Chem Int Ed 47:58–77
3. Helgesen M, Sondergaard R, Krebs FC (2010) Advanced materials and processes for polymer solar cell devices. J Mater Chem 20:36–60

4. Service RF (2011) Outlook brightens for plastic solar cells. Science 332:293
5. Cheng Y-J, Yang S-H, Hsu C-S (2009) Synthesis of conjugated polymers for organic solar cell applications. Chem Rev 109:5868–5923
6. He Y, Li Y (2011) Fullerene derivative acceptors for high performance polymer solar cells. Phys Chem Chem Phys 13:1970–1983
7. Chen J, Cao Y (2009) Development of novel conjugated donor polymers for high-efficiency bulk-heterojunction photovoltaic devices. Acc Chem Res 42:1709–1718
8. Ma W, Yang C, Gong X, Lee K, Heeger AJ (2005) Thermally stable, efficient polymer solar cells with nanoscale control of the interpenetrating network morphology. Adv Funct Mater 15:1617–1622
9. Li G, Shrotriya V, Huang J, Yao Y, Moriarty T, Emery K, Yang Y (2005) High-efficiency solution processable polymer photovoltaic cells by self-organization of polymer blends. Nat Mater 4:864–868
10. Peet J, Kim JY, Coates NE, Ma WL, Moses D, Heeger AJ, Bazan GC (2007) Efficiency enhancement in low-bandgap polymer solar cells by processing with alkane dithiols. Nat Mater 6:497–500
11. Hau SK, Yip HL, Jen AKY (2010) A review on the development of the inverted polymer solar cell architecture. Polym Rev 50:474–510
12. Kim JY, Lee K, Coates NE, Moses D, Nguyen T-Q, Dante M, Heeger AJ (2007) Efficient tandem polymer solar cells fabricated by all-solution processing. Science 317:222–225
13. Chen L-M, Xu Z, Hong Z, Yang Y (2010) Interface investigation and engineering— achieving high performance polymer photovoltaic devices. J Mater Chem 20:2575–2598
14. Ma H, Yip H-L, Huang F, Jen AKY (2010) Interface engineering for organic electronics. Adv Funct Mater 20:1371–1388
15. Po R, Carbonera C, Bernardi A, Camaioni N (2011) The role of buffer layers in polymer solar cells. Energy Environ Sci 4:285–310
16. Yu G, Gao J, Hummelen JC, Wudl F, Heeger AJ (1995) Polymer photovoltaic cells: enhanced efficiencies via a network of internal donor-acceptor heterojunctions. Science 270:1789–1791
17. Hirose Y, Kahn A, Aristove VPS (1996) Chemistry, diffusion, and electronic properties of a metal/organic semiconductor contact: In/perylenetetracarboxylic dianhydride. Appl Phys Lett 68:217–219
18. Oji H, Ito E, Furuta M, Kajikawa K, Ishii H, Ouchi Y, Seki K (1999) P-sexiphenyl/metal interfaces studied by photoemission and metastable atom electron spectroscopy. J Electron Spectrosc Relat Phenom 103:517–521
19. Lögdlund M, Brédas JL (1994) Theoretical studies of the interaction between aluminum and poly(p-phenylenevinylene) and derivatives. J Chem Phys 101:4357–4364
20. Antoniadis H, Hsieh BR, Abkowitz MA, Jenekhe SA, Stolka M (1994) Photovoltaic and photoconductive properties of aluminum/poly(p-phenylene vinylene) interfaces. Synth Met 62:265–271
21. Yu G, Zhang C, Heeger AJ (1994) Dual—function semiconducting polymer devices: Light—emitting and photodetecting diodes. Appl Phys Lett 64:1540–1542
22. Yu G, Pakbaz K, Heeger AJ (1994) Semiconducting polymer diodes: large size, low cost photodetectors with excellent visible—ultraviolet sensitivity. Appl Phys Lett 64:3422–3424
23. Shaheen SE, Brabec CJ, Sariciftci NS, Padinger F, Fromherz T, Hummelen JC (2001) 2.5% efficient organic plastic solar cells. Appl Phys Lett 78:841–843
24. Limketkai BN, Baldo MA (2005) Charge injection into cathode-doped amorphous organic semiconductors. Phys Rev B 71:085207
25. Gao D, Helander MG, Wang Z-B, Puzzo DP, Greiner MT, Lu Z-H (2010) C60:Lif blocking layer for environmentally stable bulk heterojunction solar cells. Adv Mater 22:5404–5408
26. Jönsson SKM, Carlegrim E, Zhang F, Salaneck WR, Fahlman M (2005) Photoelectron spectroscopy of the contact between the cathode and the active layers in plastic solar cells: the role of lif. Jpn J Appl Phys 44:3695–3701

27. Huang J, Xu Z, Yang Y (2007) Low-work-function surface formed by solution-processed and thermally deposited nanoscale layers of cesium carbonate. Adv Funct Mater 17:1966–1973

28. Huang JS, Hou W-J, Li J-H, Li G, Yang Y (2006) Improving the power efficiency of white light-emitting diode by doping electron transport material. Appl Phys Lett 89:133509

29. Li G, Chu CW, Shrotriya V, Huang J, Yang Y (2006) Efficient inverted polymer solar cells. Appl Phys Lett 88:253503

30. Chen FC, Wu JL, Yang SS, Hsieh KH, Chen WC (2008) Cesium carbonate as a functional interlayer for polymer photovoltaic devices. J Appl Phys 103:103721

31. Wu CI, Lin CT, Chen YH, Chen MH, Lu YJ, Wu CC (2006) Electronic structures and electron-injection mechanisms of cesium-carbonate-incorporated cathode structures for organic light-emitting devices. Appl Phys Lett 88:152104

32. Chen MH, Wu CI (2008) The roles of thermally evaporated cesium carbonate to enhance the electron injection in organic light emitting devices. J Appl Phys 104:113713

33. Liao HH, Chen LM, Xu Z, Li G, Yang Y (2008) Highly efficient inverted polymer solar cell by low temperature annealing of Cs2CO3 interlayer. Appl Phys Lett 92:3–173303

34. O'Regan B, Grätzel M (1991) A low-cost, high-efficiency solar cell based on dye-sensitized colloidal tio2 films. Nature 353:737–740

35. Fujishima A, Rao TN, Tryk DA (2000) Titanium dioxide photocatalysis. J Photochem Photobiol, C 1:1–21

36. Kim JY, Kim SH, Lee HH, Lee K, Ma W, Gong X, Heeger AJ (2006) New architecture for high-efficiency polymer photovoltaic cells using solution-based titanium oxide as an optical spacer. Adv Mater 18:572–576

37. Park SH, Roy A, Beaupre S, Cho S, Coates N, Moon JS, Moses D, Leclerc M, Lee K, Heeger AJ (2009) Bulk heterojunction solar cells with internal quantum efficiency approaching 100%. Nat Photonics 3:297–303

38. Park M-H, Li J-H, Kumar A, Li G, Yang Y (2009) Doping of the metal oxide nanostructure and its influence in organic electronics. Adv Funct Mater 19:1241–1246

39. Roest AL, Kelly JJ, Vanmaekelbergh D, Meulenkamp EA (2002) Staircase in the electron mobility of a ZnO quantum dot assembly due to shell filling. Phys Rev Lett 89:036801

40. Yip H-L, Hau SK, Baek NS, Ma H, Jen AKY (2008) Polymer solar cells that use self-assembled-monolayer- modified ZnO/metals as cathodes. Adv Mater 20:2376–2382

41. Gilot J, Barbu I, Wienk MM, Janssen RAJ (2007) The use of ZnO as optical spacer in polymer solar cells: Theoretical and experimental study. Appl Phys Lett 91:113520–113523

42. Monson TC, Lloyd MT, Olson DC, Lee Y-J, Hsu JWP (2008) Photocurrent enhancement in polythiophene- and alkanethiol-modified ZnO solar cells. Adv Mater 20:4755–4759

43. Salomon A, Berkovich D, Cahen D (2003) Molecular modification of an ionic semiconductor-metal interface: ZnO/molecule/Au diodes. Appl Phys Lett 82:1051–1053

44. Yip HL, Hau SK, Baek NS, Jen AKY (2008) Self-assembled monolayer modified ZnO/metal bilayer cathodes for polymer/fullerene bulk-heterojunction solar cells. Appl Phys Lett 92:3–193313

45. Zhang F, Ceder M, Inganäs O (2007) Enhancing the photovoltage of polymer solar cells by using a modified cathode. Adv Mater 19:1835–1838

46. Huang F, Wu H, Cao Y (2010) Water/alcohol soluble conjugated polymers as highly efficient electron transporting/injection layer in optoelectronic devices. Chem Soc Rev 39:2500–2521

47. Hoven CV, Garcia A, Bazan GC, Nguyen T-Q (2008) Recent applications of conjugated polyelectrolytes in optoelectronic devices. Adv Mater 20:3793–3810

48. Luo J, Wu HB, He C, Li AY, Yang W, Cao Y (2009) Enhanced open-circuit voltage in polymer solar cells. Appl Phys Lett 95:043301–043303

49. He C, Zhong CM, Wu HB, Yang RQ, Yang W, Huang F, Bazan GC, Cao Y (2010) Origin of the enhanced open-circuit voltage in polymer solar cells via interfacial modification using conjugated polyelectrolytes. J Mater Chem 20:2617–2622

50. Na S-I, Oh S-H, Kim S-S, Kim D-Y (2009) Efficient organic solar cells with polyfluorene derivatives as a cathode interfacial layer. Org Electron 10:496–500

51. Zhao Y, Xie Z, Qin C, Qu Y, Geng Y, Wang L (2009) Enhanced charge collection in polymer photovoltaic cells by using an ethanol-soluble conjugated polyfluorene as cathode buffer layer. Sol Energy Mater Sol Cells 93:604–608

52. Oh S-H, Na S-I, Jo J, Lim B, Vak D, Kim D-Y (2010) Water-soluble polyfluorenes as an interfacial layer leading to cathode-independent high performance of organic solar cells. Adv Funct Mater 20:1977–1983

53. Zhang LJ, He C, Chen JW, Yuan P, Huang LA, Zhang C, Cai WZ, Liu ZT, Cao Y (2010) Bulk-heterojunction solar cells with benzotriazole-based copolymers as electron donors: largely improved photovoltaic parameters by using PFN/A1 bilayer cathode. Macromolecules 43:9771–9778

54. He Z, Zhang C, Xu X, Zhang L, Huang L, Chen J, Wu H, Cao Y (2011) Largely enhanced efficiency with a PFN/A1 bilayer cathode in high efficiency bulk heterojunction photovoltaic cells with a low bandgap polycarbazole donor. Adv Mater 23:3086–3089

55. Xu X, Cai W, Chen J, Cao Y (2011) Conjugated polyelectrolytes and neutral polymers with poly(2,7-carbazole) backbone: Synthesis, characterization, and photovoltaic application. J Polym Sci Part A: Polym Chem 49:1263–1272

56. Seo JH, Gutacker A, Sun Y, Wu H, Huang F, Cao Y, Scherf U, Heeger AJ, Bazan GC (2011) Improved high-efficiency organic solar cells via incorporation of a conjugated polyelectrolyte interlayer. J Am Chem Soc 133:8416–8419

57. Zuo L, Jiang X, Xu M, Yang L, Nan Y, Yan Q, Chen H (2011) Enhancement of short current density in polymer solar cells with phthalocyanine tin (iv) dichloride as interfacial layer. Sol Energy Mater Sol Cells 95:2664–2669

58. Wei Q, Nishizawa T, Tajima K, Hashimoto K (2008) Self-organized buffer layers in organic solar cells. Adv Mater 20:2211–2216

59. Yamakawa S, Tajima K, Hashimoto K (2009) Buffer layer formation in organic photovoltaic cells by self-organization of poly(dimethylsiloxane)s. Org Electron 10:511–514

60. Mihailetchi VD, Koster LJA, Hummelen JC, Blom PWM (2004) Photocurrent generation in polymer-fullerene bulk heterojunctions. Phys Rev Lett 93:216601

61. Yuan Y, Reece TJ, Sharma P, Poddar S, Ducharme S, Gruverman A, Yang Y, Huang J (2011) Efficiency enhancement in organic solar cells with ferroelectric polymers. Nat Mater 10:296–302

62. Zhang F, Johansson M, Andersson MR, Hummelen JC, Inganäs O (2002) Polymer photovoltaic cells with conducting polymer anodes. Adv Mater 14:662–665

63. Lim YF, Lee S, Herman DJ, Lloyd MT, Anthony JE, Malliaras GG (2008) Spray-deposited poly(3,4-ethylenedioxythiophene):poly(styrenesulfonate) top electrode for organic solar cells. Appl Phys Lett 93:193301–193303

64. de Jong MP, van IJzendoorn LJ, de Voigt MJA (2000) Stability of the interface between indium-tin oxide and poly(3,4-ethylenedioxythiophene)/poly(styrenesulphonate) in polymer light-emitting diodes. Appl Phys Lett 77:2255–2257

65. Kim Y-H, Lee S-H, Noh J, Han S-H (2006) Performance and stability of electroluminescent device with self-assembled layers of poly(3,4-ethylenedioxythiophene)-poly(styrenesulfonate) and polyelectrolytes. Thin Sol Fi 510:305–310

66. Wong KW, Yip HL, Luo Y, Wong KY, Lau WM, Low KH, Chow HF, Gao ZQ, Yeung WL, Chang CC (2002) Blocking reactions between indium-tin oxide and poly (3,4-ethylene dioxythiophene): Poly(styrene sulphonate) with a self-assembly monolayer. Appl Phys Lett 80:2788–2790

67. Yan H, Lee P, Armstrong NR, Graham A, Evmenenko GA, Dutta P, Marks TJ (2005) High-performance hole-transport layers for polymer light-emitting diodes. Implementation of organosiloxane cross-linking chemistry in polymeric electroluminescent devices. J Am Chem Soc 127:3172–3183

68. Xiao T, Cui W, Anderegg J, Shinar J, Shinar R (2011) Simple routes for improving polythiophene: fullerene-based organic solar cells. Org Electron 12:257–262
69. Peng B, Guo X, Cui CH, Zou YP, Pan CY, Li YF (2011) Performance improvement of polymer solar cells by using a solvent-treated poly(3,4-ethylenedioxythiophene):poly(styrenesulfonate) buffer layer. Appl Phys Lett 98:3–243308
70. Shrotriya V, Li G, Yao Y, Chu CW, Yang Y (2006) Transition metal oxides as the buffer layer for polymer photovoltaic cells. Appl Phys Lett 88:3–073508
71. Kim DY, Subbiah J, Sarasqueta G, So F, Ding HJ, Irfan, Gao YL (2009) The effect of molybdenum oxide interlayer on organic photovoltaic cells. Appl Phys Lett 95:3–093304
72. Sun Y, Takacs CJ, Cowan SR, Seo JH, Gong X, Roy A, Heeger AJ (2011) Efficient, air-stable bulk heterojunction polymer solar cells using moO_x as the anode interfacial layer. Adv Mater 23:2226–2230
73. Irwin MD, Buchholz B, Hains AW, Chang RPH, Marks TJ (2008) P-type semiconducting nickel oxide as an efficiency-enhancing anode interfacial layer in polymer bulk-heterojunction solar cells. Proc Natl Acad Sci USA 105:2783–2787
74. Irwin MD, Servaites JD, Buchholz DB, Leever BJ, Liu J, Emery JD, Zhang M, Song J-H, Durstock MF, Freeman AJ, Bedzyk MJ, Hersam MC, Chang RPH, Ratner MA, Marks TJ (2011) Structural and electrical functionality of nio interfacial films in bulk heterojunction organic solar cells. Chem Mater 23:2218–2226
75. Steirer KX, Chesin JP, Widjonarko NE, Berry JJ, Miedaner A, Ginley DS, Olson DC (2010) Solution deposited nio thin-films as hole transport layers in organic photovoltaics. Org Electron 11:1414–1418
76. Han S, Shin WS, Seo M, Gupta D, Moon S-J, Yoo S (2009) Improving performance of organic solar cells using amorphous tungsten oxides as an interfacial buffer layer on transparent anodes. Org Electron 10:791–797
77. Yoon WJ, Berger PR (2008) 4.8% efficient poly(3-hexylthiophene)-fullerene derivative (1:0.8) bulk heterojunction photovoltaic devices with plasma treated AgOx/indium tin oxide anode modification. Appl Phys Lett 92:3–013306
78. Hains AW, Marks TJ (2008) High-efficiency hole extraction/electron-blocking layer to replace poly(3,4-ethylenedioxythiophene): Poly(styrene sulfonate) in bulk-heterojunction polymer solar cells. Appl Phys Lett 92:3–023504
79. Hains AW, Liu J, Martinson ABF, Irwin MD, Marks TJ (2010) Anode interfacial tuning via electron-blocking/hole-transport layers and indium tin oxide surface treatment in bulk-heterojunction organic photovoltaic cells. Adv Funct Mater 20:595–606
80. Subbiah J, Kim DY, Hartel M, So F (2010) MoO3/poly(9,9-dioctylfluorene-co-N-[4-(3-methylpropyl)]-diphenylamine) double-interlayer effect on polymer solar cells. Appl Phys Lett 96:3–063303
81. Li C-Y, Wen T-C, Guo T-F (2008) Sulfonated poly(diphenylamine) as a novel hole-collecting layer in polymer photovoltaic cells. J Mater Chem 18:4478–4482
82. Kang B, Tan LW, Silva SRP (2008) Fluoropolymer indium-tin-oxide buffer layers for improved power conversion in organic photovoltaics. Appl Phys Lett 93:133302–133303
83. Campoy-Quiles M, Ferenczi T, Agostinelli T, Etchegoin PG, Kim Y, Anthopoulos TD, Stavrinou PN, Bradley DDC, Nelson J (2008) Morphology evolution via self-organization and lateral, and vertical diffusion in polymer: fullerene solar cell blends. Nat Mater 7:158–164
84. Xu Z, Chen LM, Yang GW, Huang CH, Hou JH, Wu Y, Li G, Hsu CS, Yang Y (2009) Vertical phase separation in poly(3-hexylthiophene):fullerene derivative blends and its advantage for inverted structure solar cells. Adv Funct Mater 19:1227–1234
85. Liang CW, Su WF, Wang LY (2009) Enhancing the photocurrent in poly(3-hexylthiophene)/[6,6]-phenyl C-61 butyric acid methyl ester bulk heterojunction solar cells by using poly(3-hexylthiophene) as a buffer layer. Appl Phys Lett 95:3–133303
86. Zheng Q, Fang G, Bai W, Sun N, Qin P, Fan X, Cheng F, Yuan L, Zhao X (2011) Efficiency improvement in organic solar cells by inserting a discotic liquid crystal. Sol Energy Mater Sol Cells 95:2200–2205

87. Sun Y, Wang M, Gong X, Seo JH, Hsu BBY, Wudl F, Heeger AJ (2011) Polymer bulk heterojunction solar cells: function and utility of inserting a hole transport and electron blocking layer into the device structure. J Mater Chem 21:1365–1367

88. Sgobba V, Guldi DM (2008) Carbon nanotubes as integrative materials for organic photovoltaic devices. J Mater Chem 18:153–157

89. Chaudhary S, Lu H, Müller AM, Bardeen CJ, Ozkan M (2007) Hierarchical placement and associated optoelectronic impact of carbon nanotubes in polymer-fullerene solar cells. Nano Lett 7:1973–1979

90. Hatton RA, Blanchard NP, Tan LW, Latini G, Cacialli F, Silva SRP (2009) Oxidised carbon nanotubes as solution processable, high work function hole-extraction layers for organic solar cells. Org Electron 10:388–395

91. Kim JS, Park JH, Lee JH, Jo J, Kim D-Y, Cho K (2007) Control of the electrode work function and active layer morphology via surface modification of indium tin oxide for high efficiency organic photovoltaics. Appl Phys Lett 91:112111–112113

92. Hau SK, Yip H-L, Leong K, Jen AK-Y (2009) Spraycoating of silver nanoparticle electrodes for inverted polymer solar cells. Org Electron 10:719–723

93. Zeng W, Wu H, Zhang C, Huang F, Peng J, Yang W, Cao Y (2007) Polymer light-emitting diodes with cathodes printed from conducting ag paste. Adv Mater 19:810–814

94. Zhao DW, Liu P, Sun XW, Tan ST, Ke L, Kyaw AKK (2009) An inverted organic solar cell with an ultrathin ca electron-transporting layer and MoO3 hole-transporting layer. Appl Phys Lett 95:3–153304

95. Zhou Y, Cheun H, Postcavage WJ Jr, Fuentes-Hernandez C, Kim S-J, Kippelen B (2010) Inverted organic solar cells with ITO electrodes modified with an ultrathin Al2O3 buffer layer deposited by atomic layer deposition. J Mater Chem 20:6189–6194

96. White MS, Olson DC, Shaheen SE, Kopidakis N, Ginley DS (2006) Inverted bulk-heterojunction organic photovoltaic device using a solution-derived ZnO underlayer. Appl Phys Lett 89:3–143517

97. Sun YM, Seo JH, Takacs CJ, Seifter J, Heeger AJ (2011) Inverted polymer solar cells integrated with a low temperature-annealed sol-gel-derived ZnO film as an electron transport layer. Adv Mater 23:1679–1683

98. Yang TB, Cai WZ, Qin DH, Wang EG, Lan LF, Gong X, Peng JB, Cao Y (2009) Solution-processed zinc oxide thin film as a buffer layer for polymer solar cells with an inverted device structure. J Phys Chem C 114:6849–6853

99. Waldauf C, Morana M, Denk P, Schilinsky P, Coakley K, Choulis SA, Brabec CJ (2006) Highly efficient inverted organic photovoltaics using solution based titanium oxide as electron selective contact. Appl Phys Lett 89:3–233517

100. Steim R, Choulis SA, Schilinsky P, Brabec CJ (2008) Interface modification for highly efficient organic photovoltaics. Appl Phys Lett 92:3–093303

101. Oh H, Krantz J, Litzov I, Stubhan T, Pinna L, Brabec CJ (2011) Comparison of various sol-gel derived metal oxide layers for inverted organic solar cells. Sol Energy Mater Sol Cells 95:2194–2199

102. Stubhan T, Oh H, Pinna L, Krantz J, Litzov I, Brabec CJ (2011) Inverted organic solar cells using a solution processed aluminum-doped zinc oxide buffer layer. Org Electron 12:1539–1543

103. Hau SK, Yip H-L, Baek NS, Zou J, O'Malley K, Jen AKY (2008) Air-stable inverted flexible polymer solar cells using zinc oxide nanoparticles as an electron selective layer. Appl Phys Lett 92:253301–253303

104. Chua L-L, Zaumseil J, Chang J-F, Ou ECW, Ho PKH, Sirringhaus H, Friend RH (2005) General observation of n-type field-effect behaviour in organic semiconductors. Nature 434:194–199

105. Hau SK, Yip HL, Ma H, Jen AKY (2008) High performance ambient processed inverted polymer solar cells through interfacial modification with a fullerene self-assembled monolayer. Appl Phys Lett 93:3–233304

106. Hau SK, Cheng Y-J, Yip H-L, Zhang Y, Ma H, Jen AK-Y (2011) Effect of chemical modification of fullerene-based self-assembled monolayers on the performance of inverted polymer solar cells. ACS Appl Mater Interfaces 2:1892–1902

107. Khodabakhsh S, Sanderson BM, Nelson J, Jones TS (2006) Using self-assembling dipole molecules to improve charge collection in molecular solar cells. Adv Funct Mater 16:95–100

108. Armstrong NR, Carter C, Donley C, Simmonds A, Lee P, Brumbach M, Kippelen B, Domercq B, Yoo S (2003) Interface modification of ITO thin films: organic photovoltaic cells. Thin Sol Fi 445:342–352

109. Goh C, Scully SR, McGehee MD (2007) Effects of molecular interface modification in hybrid organic-inorganic photovoltaic cells. J Appl Phys 101:114503–114512

110. Hau SK, Yip HL, Acton O, Baek NS, Ma H, Jen AKY (2008) Interfacial modification to improve inverted polymer solar cells. J Mater Chem 18:5113–5119

111. Choi H, Park JS, Jeong E, Kim G-H, Lee BR, Kim SO, Song MH, Woo HY, Kim JY (2011) Combination of titanium oxide and a conjugated polyelectrolyte for high-performance inverted-type organic optoelectronic devices. Adv Mater 23:2759–2763

112. Hsieh C-H, Cheng Y-J, Li P-J, Chen C-H, Dubosc M, Liang R-M, Hsu C-S (2010) Highly efficient and stable inverted polymer solar cells integrated with a cross-linked fullerene material as an interlayer. J Am Chem Soc 132:4887–4893

113. Cheng Y-J, Hsieh C-H, He Y, Hsu C-S, Li Y (2010) Combination of indene-c60 bis-adduct and cross-linked fullerene interlayer leading to highly efficient inverted polymer solar cells. J Am Chem Soc 132:17381–17383

114. Zhou Y, Li F, Barrau S, Tian W, Inganäs O, Zhang FL (2009) Inverted and transparent polymer solar cells prepared with vacuum-free processing. Sol Energy Mater Sol Cells 93:497–500

115. Na S-I, Kim T-S, Oh S-H, Kim J, Kim S-S, Kim D-Y (2010) Enhanced performance of inverted polymer solar cells with cathode interfacial tuning via water-soluble polyfluorenes. Appl Phys Lett 97:3–223305

116. Jo G, Na S-I, Oh S-H, Lee S, Kim T-S, Wang G, Choe M, Park W, Yoon J, Kim D-Y, Kahng YH, Lee T (2010) Tuning of a graphene-electrode work function to enhance the efficiency of organic bulk heterojunction photovoltaic cells with an inverted structure. Appl Phys Lett 97:213301–213303

117. Rider DA, Worfolk BJ, Harris KD, Lalany A, Shahbazi K, Fleischauer MD, Brett MJ, Buriak JM (2010) Stable inverted polymer/fullerene solar cells using a cationic polythiophene modified PEDOT:PSS cathodic interface. Adv Funct Mater 20:2404–2415

118. Cho N, Yip H-L, Hau SK, Chen K-S, Kim T-W, Davies JA, Zeigler DF, Jen AKY (2011) N-doping of thermally polymerizable fullerenes as an electron transporting layer for inverted polymer solar cells. J Mater Chem 21:6956–6961

119. Wang J-C, Lu C-Y, Hsu J-L, Lee M-K, Hong Y-R, Perng T-P, Horng S-F, Meng H-F (2011) Efficient inverted organic solar cells without an electron selective layer. J Mater Chem 21:5723–5728

120. Kyaw AKK, Sun XW, Jiang CY, Lo GQ, Zhao DW, Kwong DL (2008) An inverted organic solar cell employing a sol–gel derived ZnO electron selective layer and thermal evaporated MoO3 hole selective layer. Appl Phys Lett 93:3–221107

121. Tao C, Ruan SP, Zhang XD, Xie GH, Shen L, Kong XZ, Dong W, Liu CX, Chen WY (2008) Performance improvement of inverted polymer solar cells with different top electrodes by introducing a MoO3 buffer layer. Appl Phys Lett 93:193307–1993307

122. Tao C, Ruan SP, Xie GH, Kong XZ, Shen L, Meng FX, Liu CX, Zhang XD, Dong W, Chen WY (2009) Role of tungsten oxide in inverted polymer solar cells. Appl Phys Lett 94:043311–043313

123. Chan MY, Lee CS, Lai SL, Fund MK, Wong FL, Sun HY, Lau KM, Lee ST (2006) Efficient organic photovoltaic devices using a combination of exciton blocking layer and anodic buffer layer. J Appl Phys 100:094506–094504

124. Huang JS, Chou CY, Liu MY, Tsai KH, Lin WH, Lin CF (2009) Solution-processed vanadium oxide as an anode interlayer for inverted polymer solar cells hybridized with ZnO nanorods. Org Electron 10:1060–1065
125. Li CY, Wen TC, Lee TH, Guo TF, Huang JCA, Lin YC, HY J (2009) An inverted polymer photovoltaic cell with increased air stability obtained by employing novel hole/electron collecting layers. J Mater Chem 19:1643–1647
126. Dong Q, Zhou Y, Pei J, Liu Z, Li Y, Yao S, Zhang J, Tian W (2010) All-spin-coating vacuum-free processed semi-transparent inverted polymer solar cells with PEDOT: PSS anode and PAH-D interfacial layer. Org Electron 11:1327–1331
127. Sun YM, Gong X, Hsu BBY, Yip HL, Jen AKY, Heeger AJ (2010) Solution-processed cross-linkable hole selective layer for polymer solar cells in the inverted structure. Appl Phys Lett 97:193310–193313
128. Weickert J, Sun H, Palumbiny C, Hesse HC, Schmidt-Mende L (2010) Spray-deposited PEDOT: PSS for inverted organic solar cells. Sol Energy Mater Sol Cells 94:2371–2374
129. Ouyang JY, Yang Y (2006) Conducting polymer as transparent electric glue. Adv Mater 18:2141–2144
130. Huang JS, Li G, Yang Y (2008) A semi-transparent plastic solar cell fabricated by a lamination process. Adv Mater 20:415–419
131. Zhou Y, Cheun H, Choi S, Potscavage JWJ, Fuentes-Hernandez C, Kippelen B (2010) Indium tin oxide-free and metal-free semitransparent organic solar cells. Appl Phys Lett 97:3–153304
132. Lim DC, Kim YT, Shim WH, Jang A-Y, Lim J-H, Kim YD, Jeong Y, Kim YD, Lee KH (2011) Wet-chemically prepared nio layers as hole transport layer in the inverted organic solar cell. Bull Korean Chem Soc 32:1067–1070
133. Lin Y-H, Yang P-C, Huang J-S, Huang G-D, Wang I-J, Wu W-H, Lin M-Y, Su W-F, Lin C-F (2011) High-efficiency inverted polymer solar cells with solution-processed metal oxides. Sol Energy Mater Sol Cells 95:2511–2515
134. Lin MY, Sun JY, Shia CH, Chen CS, Huang YA, Yang PC, Shen YM, Lin CF (2010) The inverted polymer solar cells using cuprous oxide as a hole transportation layer, pp 1171–1174
135. Ameri T, Dennler G, Lungenschmied C, Brabec CJ (2009) Organic tandem solar cells: a review. Energy Environ Sci 2:347–363
136. Hadipour A, Boer Bd, Blom PWM (2008) Organic tandem and multi-junction solar cells. Adv Funct Mater 18:169–181
137. Hiramoto M, Suezaki M, Yokoyama M (1990) Effect of thin gold interstitial-layer on the photovoltaic properties of tandem organic solar cell. Chem Lett 19:327–330
138. Yakimov A, Forrest SR (2002) High photovoltage multiple-heterojunction organic solar cells incorporating interfacial metallic nanoclusters. Appl Phys Lett 80:1667–1669
139. Dennler G, Prall HJ, Koeppe R, Egginger M, Autengruber R, Sariciftci NS (2006) Enhanced spectral coverage in tandem organic solar cells. Appl Phys Lett 89:073502–073503
140. Drechsel J, Mannig B, Kozlowski F, Pfeiffer M, Leo K, Hoppe H (2005) Efficient organic solar cells based on a double p-i-n architecture using doped wide-gap transport layers. Appl Phys Lett 86:244102–244103
141. Colsmann A, Junge J, Kayser C, Lemmer U (2006) Organic tandem solar cells comprising polymer and small-molecule subcells. Appl Phys Lett 89:3–203506
142. Janssen AGF, Riedl T, Hamwi S, Johannes HH, Kowalsky W (2007) Highly efficient organic tandem solar cells using an improved connecting architecture. Appl Phys Lett 91:3–073509
143. Zhao DW, Sun XW, Jiang CY, Kyaw AKK, Lo GQ, Kwong DL (2008) Efficient tandem organic solar cells with an Al/MoO₃ intermediate layer. Appl Phys Lett 93:3–083305
144. Kawano K, Ito N, Nishimori T, Sakai J (2006) Open circuit voltage of stacked bulk heterojunction organic solar cells. Appl Phys Lett 88:3–073514

145. Hadipour A, Bd Boer, Wildeman J, Kooistra FB, Hummelen JC, Turbiez MGR, Wienk MM, Janssen RAJ, Blom PWM (2006) Solution-processed organic tandem solar cells. Adv Funct Mater 16:1897
146. Gilot J, Wienk MM, Janssen RAJ (2007) Double and triple junction polymer solar cells processed from solution. Appl Phys Lett 90:143512–143513
147. Sista S, Park M-H, Hong Z, Wu Y, Hou J, Kwan WL, Li G, Yang Y (2010) Highly efficient tandem polymer photovoltaic cells. Adv Mater 22:380–383
148. Park MH, Li JH, Kumar A, Li G, Yang Y (2009) Doping of the metal oxide nanostructure and its influence in organic electronics. Adv Funct Mater 19:1241–1246
149. Chou C-H, Kwan WL, Hong Z, Chen L-M, Yang Y (2011) A metal-oxide interconnection layer for polymer tandem solar cells with an inverted architecture. Adv Mater 23:1282–1286
150. Sun XW, Zhao DW, Ke L, Kyau AKK, Lo GQ, Kwang DL (2010) Inverted tandem organic solar cells with a MoO_3/Ag/Al/Ca intermediate layer. Appl Phys Lett 97:3–053303